Title: Mass cytometry data integration methods reveal rural-urban gradient of immune profiles across geography

Authors: Koen A. Stam[1], Jeremia J. Pyuza[1,2], Mikhael Manurung[1], Dicky L. Tahapary[3,4], Taniawati Supali[5], Marloes M.A.R. van Dorst[1], Ahmed Mahfouz[6,7] Mohammed Charrout[7], Simon P. Jochems[1], Wesley Huisman[1], Marion König[1], Yvonne C.M. Kruize[1], Marouba Cisse[8], Ibrahima Diallo[8], Moustapha Mbow[8], Maria Yazdanbakhsh[1*], Wouter A.A. de Steenhuijsen Piters[1*]

Affiliations:

[1]LUCID, Leiden University Medical Center, 2333 ZA Leiden, Netherlands.

[2]Department of Pathology, Kilimanjaro Christian Medical Centre, Moshi, Tanzania

[3]Division of Endocrinology, Metabolism and Diabetes, Department of Internal Medicine, Cipto Mangunkusumo National Referral Hospital, Faculty of Medicine Universitas Indonesia, Jakarta, Indonesia

[4]Metabolic Disorder, Cardiovascular and Aging Research Center, The Indonesian Medical Education and Research Institute, Faculty of Medicine Universitas Indonesia, Jakarta, Indonesia

[5]Department of Parasitology, Faculty of Medicine, Universitas Indonesia, Jakarta, Indonesia

[6]Department of Human Genetics, Leiden University Medical Centre, Leiden, the Netherlands

[7]Delft Bioinformatics Lab, Delft University of Technology, Delft, The Netherlands

[8]Department of Immunology, Faculty of Medicine, Pharmacy and Odontology, Cheikh Anta Diop University of Dakar, Dakar, Senegal

* Shared last author

Correspondence to: w.desteenhuijsen@amsterdamumc.nl

ABSTRACT

The human immune system strongly varies across populations and is shaped by a wide range of host and environmental factors. As such, a rural compared to urban lifestyle has previously been associated with baseline differences in immune profiles, which can impact outcome of vaccination. The question whether there is a immune signature that associates with rural living irrespective of ancestry or geography has been addressed here along with which analytical methods are most suitable. Using three mass cytometry datasets, we studied shared and population-specific immune characteristics of healthy rural- or urban-living Indonesian, Senegalese and Tanzanian adults and urban-living Europeans. After harmonized preprocessing and quality control, 75.4 million cells were integrated using four different data-integration methods. Among these, CytoNorm with *in silico* references performed best, revealing shared differences in the differentiation state within the lymphocyte compartment that distinguishes rural from urban-living individuals. Differentiated $CD4^+$ T cells expressing CTLA-4, PD-1 and ICOS characterized rural living, as did $CD4^+$ T cells with high CD161 expression in combination with CRTH2 and GATA3. In the innate compartment, $CD56^-$ $CD16^+$ NK cells with low CD38 and CD11c expression were expanded in rural living subjects. Together, our results demonstrate that, using a harmonized analytical pipeline and machine learning-based integration, large-scale mass cytometry data can be combined across diverse cohorts to identify shared immunological hallmarks of rural living. These signatures may provide targets for modulating immune responses in future vaccine studies.

Introduction

The invention of vaccines for the prevention of infectious diseases has been one of the greatest scientific innovations. Each year, millions of deaths worldwide are prevented due to childhood immunization (Li et al., 2021). Although the use of vaccines has been a remarkable medical breakthrough, research findings from across the globe have shown striking variation in vaccine performance across different populations. Lower responses have been observed in populations living in low- and middle-income countries (LMICs) compared to high-income countries (HICs). Reduced vaccine immunogenicity, often referred to as *vaccine hypo-responsiveness*, has been described across multiple vaccine platforms (van Dorst et al., 2024), including vaccines against BCG tuberculosis, ebolavirus and yellow fever (YF) (Muyanja et al., 2014; Natukunda et al., 2024). The lower immunogenicity can translate into lower vaccine efficacy, which has been observed for among others, rotavirus and malaria vaccines. For example, attenuated malaria vaccine protects 92% of vaccinated participants in Europe (Epstein et al., 2017), but drops to 27% in Africa (Sissoko et al., 2017),

Pre-vaccination immune signature profiles play a critical role in shaping vaccine responsiveness (Fourati et al., 2022; Hagan et al., 2022; HIPC-CHI Signatures Project Team & HIPC-I Consortium, 2017; Kotliarov et al., 2020; Tsang et al., 2014). For example, a study revealed a shared pro-inflammatory transcriptional signature linked to higher serum antibody responses one month post-vaccination across 13 vaccines (Fourati et al., 2022). Of note, these integrative studies are mainly based on blood transcriptional profiles of healthy individuals living in HICs, lacking data on populations in LMICs. Even within LMICs, baseline immune activation and as such vaccine-induced immune responses vary (Temba et al., 2021). A recent study on Tanzanian adults showed that urban living was related to a stronger pro-inflammatory profile compared to individuals adopting a rural lifestyle (Temba et al., 2021).

Baseline immune state is shaped by a range of factors, including age, heritable (genetics) and non-heritable factors (e.g. vaccination, nutrition (Temba et al., 2021), CMV or helminth infections, epigenetics and microbiota composition) (Brodin & Davis, 2017; Brodin et al., 2015) In particular, non-heritable and lifestyle factors co-occur with the degree of urbanization, possibly explaining

differences in baseline immune signatures and responsiveness to vaccines. Immune profiles related to helminth-infected, rural-living Indonesians were characterized by expanded frequencies of T helper 2 and regulatory T cells expressing CTLA-4, a marker associated with the suppressive function of these cells. Upon deworming treatment, CTLA-4-expressing regulatory T cells in rural-living Indonesians decreased, but not reaching the low levels of uninfected European individuals. (de Ruiter et al., 2020) As baseline immune states are likely driven by a multitude of underlying factors, part of which may not even be known at this point, it is therefore important to map the immune networks of populations living along the rural-urban gradient in LMIC settings. Doing so, we may be able to divert unfavorable environmental exposures on baseline immune states by targeting the downstream immune processes. This approach would be particularly successful if immune hallmarks are shared between low-responding populations, despite the fact that environmental drivers leading to these immunological characteristics may be different.

To characterize immune profiles along the rural-urban gradient in detail, we integrated mass cytometry datasets across three studies, using different analytical methods to assess their performance. Immune profiles from 172 healthy adults from urban and rural sites (Indonesia, Tanzania and Senegal) and from an urban area in The Netherlands, were used allowing us to both assess shared and population-specific immune profiles across geography.

Results

Study participants

For this study, we included 172 participants from three studies (Senegal, CapTan and SugarSpin) conducted across four countries (Senegal, Tanzania, Indonesia and the Netherlands; Figure 1A, Table S1). All participants were healthy adults. The median age was 26 years (range, 17 – 55 years) and 52% of participants was female (Table S2). For non-European countries, samples were collected from individuals living in urban or rural areas, which previously was shown to be associated with distinct cellular immune profiles (de Ruiter et al., 2020; Manurung et al., 2025; Pyuza et al., 2024). All

98 participants had always lived in their respective residence areas. Helminth infection status was tested
99 and summarized, showing different prevalences in the rural areas (Table 1).

100

101 *Generating an integrated mass cytometry dataset accounting across studies*

102 From all individuals, PBMC samples were available, from which we profiled a total of 183 million
103 immune cells using mass cytometry and largely identical panels (Figure 1B, Table S3). Using these
104 data, we generated an integrated dataset of mass cytometry studies conducted across geographical
105 locations. First, raw (bead-normalized) data were preprocessed through a unified pipeline (Figure S1).
106 The resulting dataset (75.4 million cells) was used without further preprocessing ('raw') or were
107 subjected to within-study batch-correction using CytoNorm (CN_{within}) or between-study batch-
108 correction (CytofIn (Lo et al., 2022), Harmony (Korsunsky et al., 2019), quantile or
109 CytoNorm[$CN_{between}$] (Van Gassen et al., 2020)). Global differences in the performance of integration
110 methods were visualized using t-distributed Stochastic Neighbor Embedding (t-SNE). These t-SNE-
111 plots clearly underscored the need for data-integration methods, revealing strong separation according
112 to cell lineage and study in non-integrated and within-study batch-adjusted datasets. In contrast, batch
113 effects (largely) disappeared in the integrated datasets (CytofIn, Harmony, quantile and $CN_{between}$), and
114 cells mostly separated based on cell lineage (Figure 1D-E).

115

116 To quantify integration performance in more detail, we calculated the local inverse Simpson index
117 (LISI), which is a diversity score that measures how well studies are mixed in the local neighborhood
118 of each cell (Korsunsky et al., 2019). LISI showed marked differences between integration methods,
119 with the highest median LISI-scores in $CN_{between}$-adjusted data (median 2.39, IQR 2.08-2.67; Figure
120 1F), indicating superior integration compared to other methods. Similarly, *k*-nearest-neighbor batch-
121 effect test (kBET)-scores indicated best integration was reached for the $CN_{between}$-adjusted data (Figure
122 S2).

123

Automated annotation of cell clusters and comparisons before and after integration

Given the superior integration metrics, we decided to proceed with the $CN_{between}$-adjusted data for downstream analyses. Data were clustered using self-organizing maps (SOM; 15 × 15 grid) and meta-clustering was performed for a range of *k*-values (total number of clusters). Based on cluster-level inverse Simpson indices (ISI) across European samples, we determined that the optimal number of clusters was k = 125, balancing a peak in the ISI score with a high number of clusters to capture granular differences in the immune system (first local peak in median ISI across clusters with k ≥ 100; Figures S3 and S4). As a first exploratory analysis, we performed principal component analysis (PCA) on the cluster frequencies. The first two principal components explained 16.1% of the variance in the data (Figure 1G). Strongest separation was observed along the first principal component, where Europeans clearly clustered apart from non-Europeans, which was verified using PERMANOVA-tests (R^2 = 8.9%, *p*-value = 0.0001, permutations restricted within study strata). Despite this, a residual effect of study ID was visible, mostly along the second principal component (PERMANOVA R^2 = 5.4%, *p*-value = 0.0001). We next assessed overall cell cluster diversity, both assessing the number of clusters present at cell frequency > 0.1% and the evenness of the distribution of these clusters. We found that rural-living individuals overall have a more diverse immune profile compared to both urban-living non-Europeans and Europeans (Shannon index; linear model, adjusting for study; *q*-value 0.01 and 1.6×10^{-10}, respectively; Figure S5A), which was particularly apparent in the $CD4^+$ T cell compartment (Figure S5B). This difference may be explained by higher variation in environmental exposures related to rural lifestyle, resulting in a more heterogeneous immune cell signature in rural living individuals.

Next, cell clusters were annotated using an automated and standardized marker-based algorithm. In brief, the algorithm derives for each cluster whether a given marker is positive, negative or neutral, based on the intensity distribution across all clusters for that marker. For each cluster a label is assigned based on a set of predefined 'rules' (Table S4). To assess the effect of integration on cell type annotations, we employed the automatic annotation scheme to both the unintegrated and

151 integrated data. We assessed the effect of the integration and the ability to preserve biology by
152 comparing cell type annotation of the integrated data to the unintegrated data using the F1-measure
153 (Figure 2A-C). The effects of integration with $CN_{between}$ were minimal at the lineage level, with the
154 median F1-measure (measure for accuracy of cell labels post-integration compared to pre-integration
155 labels) across lineages ranging between 0.96-0.98. However, at the subset-level, F1-measures
156 dropped, with median subset-level scores of 0.77, 0.78 and 0.82 for the CapTan, Senegal and
157 SugarSpin study, respectively (Figure 2C). We found that lower-scoring subsets, such as $CD4^+$ CM T
158 cells (F1-scores 0.66-0.73), are split across $CD4^+$ CM, EM and naive cells after integration (Figure
159 2A). Furthermore, although different CD8 T cell subsets (i.e. CD8 EM, CM and EMRA) could be
160 discerned before integration in each study, a portion of these cells were annotated as 'CD8 T cell'
161 after integration (especially in Captan and Senegal, F1-score 0.34 and 0.35, respectively). 'CD8 T
162 cell' is a general label given to cells within the CD8 T cell lineage that lack clear negative or positive
163 markers to further distinguish between specific subsets (Table S4). On the other hand, specific cell
164 phenotypes, including B cells, classical monocytes, ILC2s, and pDCs, showed consistently high F1
165 scores (>0.8) and thus good integration across all studies (Figure 2C). Of note, subsets with lower F1
166 scores were often defined by markers tagged with metal isotopes that differed between studies (e.g.
167 for CapTan, Senegal and SugarSpin studies, Gd_{155}, Pt_{198} or Cd_{113}-isotopes were conjugated to
168 CD45RA-antibodies, respectively; Table S3). This confirms that differences in panel design between
169 mass cytometry datasets poses a challenge upon data integration.

170 Next, to evaluate cell populations in the context of urban–rural differences, we manually reviewed
171 the annotations generated by the automatic cell labeler to ensure accurate and consistent phenotyping.
172 (Figure 2D, Table S5). Of the 125 clusters, 90 retained their original labels after manual review,
173 meaning no changes were made to their assigned subset or lineage. Among the remaining 35 clusters,
174 the labeler was unable to annotate 9. Of these, 2 were relabeled as "other," indicating that their
175 phenotype could not be matched to a meaningful lineage or subset (e.g., negative for all markers).
176 Consequently, only 7 of the 125 clusters required manual labeling from scratch. For the other 24
177 clusters, manual edits involved minor refinements to better specify the phenotype. For example,

178 clusters initially labeled with general categories such as “CD4 T cell” or “CD8 T cell” were updated
179 to more specific phenotypes, such as “CD8 Naive” or “CD8 EM” (Figure 2D).

180

181 *The immune composition of rural living individuals is emphasized by CD4$^+$ T cell differentiation*

182 To study variation in the immune cell composition between populations, a generalized linear mixed
183 model was used to assess how integrated immune cell populations differed between urban and rural-
184 living non-European individuals (Figure 3, Figure S6-S7). As a secondary analysis, we compared
185 immune profiles of these individuals to urban-living Europeans, hypothesizing this group would
186 represent the most urban signature, allowing us to study rural-urban differences across a collective
187 gradient. This gradient was classified based on the significance and direction of differences between
188 1) rural and urban-living non-Europeans (Ru - Ur), 2) rural-living individual non-Europeans and
189 Europeans (Ru - EU) and 3) urban-living non-Europeans and Europeans (Ur - EU). Significant
190 differences in all comparisons (1., 2. and 3.) were referred to as a ‘full urban > rural gradient’ or ‘full
191 urban < rural gradient’ depending on the direction of the effects (Figure 3A-B). Overall, we found 11
192 clusters following the full rural > urban gradient (whereby cluster frequencies were highest in rural
193 and lowest in Europeans). In contrast, none of the clusters exhibited a full urban < rural gradient
194 (Figure 3A-B). Also considering partial urban – rural gradients (comparisons 1. and 2. or 2. and 3.
195 significant) and limited urban – rural differences (comparison 1. significant), we identified in total 20
196 clusters and 3 subsets. (Figure 3D; Figure S6-S7).

197

198 Analysis of CD4$^+$ T cell clusters, showed that the T cell compartment was in a more differentiated
199 state in rural individuals. Within this compartment, three clusters of CD161$^+$ CD4 T cells (cluster 54,
200 59 and 68) were strongly associated with a rural lifestyle, showing a full rural > urban gradient
201 (Figure 3D and Figure S7). Phenotypically, these clusters were all positive for CD161 and exhibited a
202 strongly exhausted profile, expressing the immune checkpoint receptors CD279 (PD-1) and CD152

203 (CTLA-4). However, these clusters varied in expression of CD27, CD127, and CD196 (CCR6),
204 possibly indicating a different degree of antigen experience and their tissue-specific homing capacity.

205

206 The most defining difference between urban- and rural-living individuals was found within the T
207 helper (Th) 2 cell compartment. At the subset level, we found that Th2 cells, characterized by CD294
208 (CRTH2) expression, had higher frequencies in rural individuals compared to urban-living and
209 European individuals (median 0.9% vs. 0.5% and 0.3% of total $CD45^{+}$ cells, respectively; Figure S8).
210 At the cluster level, two Th2 subpopulations were identified: $GATA3^{+}CD161^{+}$ (cluster 58) and a
211 $GATA3^{dim}CD161^{-}$ population (cluster 57; Figure 3D). Cluster 58, which also showed increased
212 expression of activation markers such as CD278 (ICOS), CD279 (PD-1), and KLRG1, displayed the
213 strongest differences between rural- and urban-living individuals (Figure 3D), with smaller
214 differences between urban-living individuals and Europeans. However, cluster 57, the less
215 differentiated cluster of Th2, showed a more linear relationship across the full urban to rural gradient,
216 with larger effect sizes between groups. This linear trend may be interpreted as lifetime exposure to a
217 type 2 immunity-inducing environment.

218

219 *Urban-living individuals show higher levels of naive and $CD161^{+}$ CD8 T cells*

220 Within the $CD8^{+}$ T cell compartment, we identified eight clusters that differed significantly between
221 urban- and rural-living individuals. Two clusters were associated with rural and six were associated
222 with urban lifestyle. The differences between rural- and urban lifestyle-associated $CD8^{+}$ T cell
223 clusters were best explained by their differentiation state: $CD8^{+}$ T EM and EMRA subsets were
224 enriched in rural, whereas naïve $CD8^{+}$ T cells were enriched in urban-living individuals (Figure 3A-
225 C). The $CD8^{+}$ T cell cluster strongest associated with rural lifestyle and exhibiting a full rural > urban
226 gradient, comprised EMRA CD8+ T cells that expressed TBX21 (Tbet), but lacked CD27 and CD127
227 (cluster 6; Figure 3C-D). Similarly, we identified an EM $CD8^{+}$ T cell cluster (cluster 24) that

228 expressed T-bet and CD38, together with increased expression of CD279 (PD-1), resembling the rural
229 lifestyle–associated CD4+ T cell cluster with high PD-1 and CTLA-4 expression.

230 Naive $CD8^+$ T cell clusters showed a different pattern, for instance a cluster of naïve $CD8^+$ T cells
231 (cluster 12) was clearly lower in rural-living individuals, but had similar cell frequencies in Europeans
232 and urban living individuals (median 10.0% compared to 9.4% of total $CD45^+$ cells, respectively;
233 Figure 3D). In addition, we identified a cluster of $CD161^{bright}$ $CD8^+$ T cells, likely representing
234 mucosal-associated invariant T (MAIT) cells (cluster 49). Together with cluster 50, these cells form a
235 distinct subpopulation of $CD8^+$ T cells that is largely depleted in rural-living individuals (Figure S9).

236

237 *Mature NK and B cells are enriched in rural-living individuals*

238 In the innate part of the immune system differences between urban and rural are mostly characterized
239 by differences between NK cells. The NK (CD16) subset, compromising of two $CD16^+$ and $CD56^{dim/-}$
240 clusters, are highest in rural living individuals and are significant on the full rural urban scale (Figure
241 3D and Figure S7). More specifically, we identified a cluster (cluster 115) of $CD56^-$ $CD16^+$ $CD11c^{dim}$
242 $CD38^{dim}$ (IL2RB) NK cells, which were associated with rural lifestyle. In the Europeans, these mature
243 NK cells were only found in a small abundance (median 0.02% of total $CD45^+$). Within the non-
244 European population the median expression was respectively 0.06% and 0.17% for urban and rural
245 living individuals. In some of the rural living individuals the percentage of cluster 115 even goes
246 above 1% of total $CD45^+$ (Figure 3D). In other innate lymphoid cells, a lower frequency of ILC2s
247 could be observed in rural living individuals, characterized by their positive expression for CD25,
248 CD161 and CD294 (CRTH2). These cells were significantly different to the urban population, but not
249 the European individuals (Figure S6).

250 Other cell subsets and clusters within the innate compartment, such as monocytes and DCs, do not
251 seem to differ between urban and rural living individuals. However, the CyTOF panels used are
252 limited in defining more granular innate subsets within these immune cell populations. When
253 comparing these individuals to the Europeans, we do see clear differences. For example, the classical

254 monocytes compartment is almost twice as large in frequency than the non-European individuals. For
255 Europeans these cells comprise around 14.5% of total immune cells, whereas for non-Europeans this
256 was 8.6 %. Within the B-cell compartment, we identified a cluster of $CCR6^+$ B cells associated with
257 rural compared to urban-living (cluster 114; Figure 3D).

258

259 *Several well-integrated clusters show population specific differences*

260 To identify population-specific differences across geographical contexts (Indonesia, Tanzania, and
261 Senegal), we compared cluster-specific ISI scores using a complementary approach. ISI values were
262 first evaluated within European samples only, where they reflect integration quality, as each dataset
263 contained its own European cohort. We then compared these values to ISI scores calculated for non-
264 European samples, for which the ISI captures both integration quality and biological variation
265 between populations. A pronounced decrease in ISI in non-Europeans relative to Europeans therefore
266 indicates population-specific biological differences within otherwise well-integrated clusters.We
267 identified four cell clusters demonstrating this pattern (Figure 3E). All four clusters showed
268 significant differences between populations, with clusters of NK (CD56) $CD16^+$ $CD122^+$ $CD161^+$
269 $CD335^{dim}$ $KLRG1^+$ and $CD8^+$ EMRA $KLRG1^{dim}$ specifically enriched in Indonesians. The increased
270 frequency of CD4 EM and naive $CD127^+$ $CD27^+$ cells in Tanzanian and Senegalese participants
271 compared to their Indonesian counterparts underscores significant geographical differences in
272 immune cell distribution (Figure S10).

273

274 *The cellular immune signature can be used to robustly predict living location*

275 To capture immune differences beyond the clusters identified by the linear mixed models, we next
276 applied a multivariate modeling approach to predict urban versus rural living. This strategy allowed us
277 to assess the combined predictive value of immune cell composition and functional state. Guided by
278 the observed differences in activation and differentiation, particularly within $CD4^+$ and $CD8^+$ T cell
279 compartments, we constructed an integrated immune feature set for classification.

This feature set comprised an overall immune diversity (Shannon index), relative frequencies of 26 cellular subsets, and the 80th percentile expression of eight key activation markers calculated at the subset level, yielding 235 features per individual. The use of high-quantile marker expression captured activation states while remaining robust to outliers. All features were derived from automatically annotated cell subsets, minimizing bias from manual gating or subjective cell labeling. Using this integrated immune signature, we trained machine learning models that robustly discriminated between urban and rural living within the non-European cohort.

Across nine machine learning models, seven achieved a median training accuracy greater than 0.60, indicating moderate to good performance while maintaining generalizability (Figure 4A). The best-performing model, the Lasso and Elastic-net regularized generalized linear model (glmnet), consistently showed stable training accuracy and the highest test accuracy of 0.70. Notably, the model's feature selection reinforced key biological insights, among the top twelve most selected features, one represented a cellular subset frequency (Th2 *frequency*). Confirming the results from the generalized linear mixed models and its ability to distinguishing between urban and rural lifestyles.

The other eleven features were activation markers, highlighting that expression and differentiation state of immune subsets are dominant predictive factors (Figure 4B). For instance, KLRG1 expression on Th2 cells was strongly associated with rural living, whereas higher CD197 (CCR7) expression correlated with urban environments. The single most predictive feature, selected 100% of the time, was CD152 (CTLA4) expression on CD4 central memory cells, suggesting a link between rural living and sustained antigenic exposure. Additionally, CD196 (CCR6) emerged as a key marker, appearing four times among the top predictors. Elevated CCR6 expression on CD4 effector memory T cells, B cells, and dendritic cells was characteristic of an urban profile, while its expression on plasmacytoid dendritic cells was more indicative of a rural lifestyle. Together, these results suggest that differences in immune activation status and memory phenotypes, rather than cell frequencies alone, are key determinants of the immune signature associated with urban versus rural living, consistent with the patterns observed in the cluster-wise linear mixed models.

307 **Discussion**

308 In this study, we used three mass cytometry datasets to study shared- and study-specific effects in
309 immune signatures among Europeans and non-European rural- and urban-living individuals. We
310 applied and benchmarked data-integration methods, finding strong differences in integration quality
311 between methods. Using the top-performing integration method we were able to assess in detail
312 cellular immune profiles associated with rural- or urban-living location shared across geography.
313 Generally, rural-living individuals showed an immune profile that was marked by an overall highly
314 differentiated and activated state. Using machine learning models, we were able to discriminate rural-
315 and urban-living individuals based on these profiles with moderate to high accuracy.

316

317 In literature, several methods for batch normalization within mass cytometry datasets have been
318 proposed, including quantile and CytoNorm normalization. CytoNorm (Van Gassen et al., 2020)
319 performs a cluster-specific batch-adjustment for each marker by aligning identical technical replicates
320 towards a predefined goal distribution, allowing for cell type specific marker intensity adjustments.
321 However, existing datasets typically lack shared technical replicates, hampering the use of this
322 method for between-study batch-correction. Here, we showed this issue can be solved by generating
323 an *in silico* reference sample through subsampling cells across study groups, resulting in superior
324 integration metrics. Other methods, notably CytofIn (Lo et al., 2022), despite abrogating the need for
325 shared technical replicates between studies, performed less well based on LISI scores. Methods
326 applied in the single-cell sequencing field (Luecken et al., 2022), including Harmony (Korsunsky et
327 al., 2019), also showed lower performance and typically do not scale well across 10s to 100s of
328 millions of cells. The ability to preserve cell labels before and after integration was additionally used
329 as a measure of data integration. Automatic cell labels were preserved at lineage level, but
330 performance diminished at subset or cluster level, which is in line with previous work assessing cell
331 population identification algorithms (Abdelaal et al., 2019). Nonetheless, the automatic cell labeler
332 was a highly suitable tool for assisting in phenotyping immune cells and represented a step forward in
333 harmonizing cell type annotations across studies. This labor-intensive work often demands profound

334 immunological expertise and is an essential prerequisite for understanding immune cell diversity and
335 functionality (Li et al., 2025).

336

337 Our data showed an overall relative enlargement of the memory pool within the $CD4^+$ and $CD8^+$ T
338 cell lineages in non-European rural- compared to urban-living non-Europeans and Europeans, which
339 is in line with previous findings. Among others, previous work in Senegalese urban- and rural-living
340 participants showed higher frequencies of memory $CD4^+$ T and B cells (Manurung et al., 2025; Mbow
341 et al., 2014). We also confirm a strong Th2 polarization in rural-living individuals (de Ruiter et al.,
342 2020) and highlight that the largest difference to urban living individuals is within the Th2 cell
343 population that show a more differentiated phenotype, characterized by CD161 expression. These
344 $CD161^+$ $GATA3^+$ Th2 cells, previously recognized as pathogenic effect Th2 (peTh2) cells, are
345 thought to be driven by chronic antigen exposure and have an enhanced effector function (Gazzinelli-
346 Guimaraes et al., 2024; Mitson-Salazar et al., 2016). Whereas the difference in these peTh2 cell
347 frequencies between urban and rural-living individuals is striking, the difference between non-
348 European and European urban-living individuals is very subtle, suggesting that indeed adopting an
349 urban lifestyle is linked to a reduction in Th2 inducing antigenic exposures. Contrary to peTh2 cells,
350 conventional Th2 cells (cTh2) show a very gradual increase of expression across the full urban to
351 rural gradient, which might reflect more the lifetime exposure to Th2 inducing environment.

352

353 The increased expression of C-type lectin-like receptor CD161 in rural-living individuals was not
354 limited to Th2 cells, but also emerged on other $CD4^+$ T cells, both in the effector and central memory
355 compartment. For example, one cluster of $CD4^+$ $CD127^{++}$ $CD161^+$ was strongly associated with rural-
356 living individuals and showing a clear trend across the full urban rural gradient. The bright expression
357 of the interleukin-7 receptor (CD127) can be interpreted as another indication of continuous exposure
358 to an environment rich in microorganisms and parasites (Mazzucchelli & Durum, 2007). Furthermore,
359 $CD161^+$ $CD4^+$ T EM cells have previously been associated with naturally acquired immunity against

360 malaria in endemic areas, and could be induced after repeated exposure to malaria (de Jong et al.,
361 2021). In addition, tumor-infiltrating CD161^{+} EM CD4^{+} T cells are associated with improved survival
362 in human papillomavirus (HPV)16-associated tumors and could be induced through therapeutic
363 vaccination with HPV16 vaccine (Duurland et al., 2022), which might support a role for these cells in
364 immunity. Similarly, higher CTLA-4 (CD152) was more strongly expressed in both central and
365 effector memory CD4+ T cells in rural-living individuals, which was most apparent in our prediction
366 model results. CTLA-4 is constitutively expressed in regulatory T cells, but also upregulated in
367 conventional T cells after activation. This could result from repeated antigenic stimulation, which is
368 likely to lead to immune exhaustion and, in turn, increased expression of inhibitory receptors such as
369 CTLA-4 and PD-1 (van Dorst et al., 2024). The programmed cell death protein (PD-1) was indeed
370 one of the other exhaustion markers that showed increased expression across the different immune
371 lineages captured by several clusters that were increased in rural living individuals, including CD8
372 EM, CD4 EM, Th2 cells and Tregs.

373

374 Whereas CD161 expression on CD4^{+} T-cells appears to be a hallmark of individuals living in rural
375 settings, the opposite is true for CD8^{+} T cells. Both from the univariate analysis and prediction
376 models, CD161 expression on CD8 T cells is strongly associated with urban-living individuals. We
377 identified two clusters of CD161^{bright} CD8^{+} T cells, which could be considered as mucosal-associated
378 invariant T (MAIT) cells, but should be validated by identifying the presence of an invariant T cell
379 receptor (Vα7.2). Both these clusters were lower in rural- compared to urban-living individuals and
380 highest in European individuals. Abundance of MAIT cells varies widely among people and is
381 particularly low in people at high risk of disease, including the very young, the elderly and the
382 immunocompromised (Godfrey et al., 2019).

383

384 Within the innate immune system, we identified a cluster of CD56^{-} CD16^{+} CD11c^{dim} NK cells being
385 elevated, with the second highest effect size, in rural living individuals. It is suggested that these cells

386 are induced by chronic disease, and that individuals with these NK cells could respond differently to
387 NK-mediated immunotherapies, infections or vaccines (Forconi et al., 2020). From the machine
388 learning models we found that the expression of CD196 (CCR6) on plasmacytoid dendritic cells
389 (pDCs) was lower in urban-living individuals, while it was higher in other dendritic cell clusters
390 (DCs). CCR6 (CD196) and its ligand CCL20 can be related to several lung and gut disorders and play
391 an important role in mucosal immunity (Ito et al., 2011). The observed variation in CCR6 expression
392 across DC subsets could influence the behavior and function of these cells and may reveal
393 mechanisms by which vaccines elicit different immune responses across populations.

394

395 This is the first study aimed at integrating mass cytometry data across healthy individuals living
396 across the European-non-European urban-rural gradient. However, there are several limitations in our
397 study. First, data integration will always be a balancing act between removing study-specific effects
398 versus preserving biological signals. Therefore, even after integration, we retrieve study-specific cell
399 clusters, which could signal either suboptimal integration or true population-specific effects.
400 Leveraging the availability of samples from European individuals in each study, we tried to
401 discriminate between these scenarios. Second, the addition of new data would require rerunning the
402 normalization and clustering algorithms. However, through relatively simple adjustments, for example
403 by defining the goal distribution as the reference of a given study or current set of studies, we could
404 make this an expandable dataset.

405 Factors underlying immune variation between urban and rural lifestyle include diet (Temba et al.,
406 2021), CMV and parasitic infections (de Ruiter et al., 2020), (early life) microbial exposures and
407 resulting epigenetic changes, and differences in microbiota composition (Pyuza et al., 2025; Strazar et
408 al., 2021)- and microbiome-derived metabolites (Temba et al., 2021). Importantly, these factors may
409 vary between rural populations, although the downstream immunological effects predisposing to
410 altered vaccine responsiveness may in fact be the same. This work underlines this idea, mainly
411 identifying shared immunological hallmarks between genetically distinct rural populations. As such,
412 these hallmarks may serve as targets for further prevention or intervention studies.

413

414 **Methods**

415 *Study design*

416 Healthy adults living in rural and urban areas (Senegal, Tanzania and Indonesia) and in urban areas in
417 the Netherlands were included in this study.

418 Details on study design and in-/exclusion criteria on the study conducted in Indonesia ('SugarSpin')
419 were published previously (de Ruiter et al., 2020; Tahapary et al., 2015). In short, the Indonesian
420 samples were part of the SUGARSPIN trial, a household-based cluster-randomized double-blind trial
421 that was conducted in three rural villages in Nangapanda, Flores Island, Indonesia. The trial was
422 approved by the ethics committee of the Faculty of Medicine, Universitas Indonesia (FKUI)
423 (reference no. 549/H2·F1/ETIK/2013) and filed by the ethics committee of Leiden University Medical
424 Center (LUMC). The trial is registered as a clinical trial (reference no. ISRCTN75636394). Written
425 informed consent was obtained from participants before the study. Age- and sex-matched samples of
426 healthy volunteers from The Netherlands or from urban centers in Indonesia, including central
427 Jakarta, without helminth infections were additionally included.

428 For the 'Senegal' study, details on the study were previously published (Manurung et al., 2025). In
429 short, samples were collected from healthy Senegalese adults living in rural (Pakh and Richard-Toll)
430 and urban (Dakar) areas and in urban areas in The Netherlands. Participants were included in the trial
431 if they had been living in their respective residence areas for ≥10 years, preferably lifelong, were 18-
432 40 years of age, did not have chronic diseases, and tested negative for schistosomiasis and malaria.

433 Samples from healthy Tanzanian adults were collected in the context of the 'CapTan' trial, aimed at
434 assessing differences in immunogenicity of the yellow fever vaccine between urban and rural-living
435 individuals. Details on the study conducted were previously published (Pyuza et al., 2024). To
436 summarize, the study was approved by the Ethical Board of the Kilimanjaro Christian Medical
437 University College (No. 2588) and by the Tanzania National Ethical Committee Board
438 (NIMR/HQ/R.8a/Vol.IX/4089). Samples were collected from two rural areas (Upper Moshi and
439 Mwanga) and two urban areas (Lower Moshi and Arusha). In addition, healthy adults living in an

440 urban area in The Netherlands were included, which were part of the 'TINO'- study
441 (ClinicalTrials.gov, reference no. NCT06039527). The study was approved by the Ethics Committee
442 of Leiden University Medical Center (NL77841.058.21).

443

444 *Parasitology*

445 Fresh stool samples of rural Indonesian, Tanzanian and Senegalese rural-/urban-living adults were
446 microscopically screened for soil-transmitted helminth infections (hookworms, *Ascaris lumbricoides*,
447 *Trichuris trichiura* by Kato-Katz. Tanzanian and Senegalese adults were additionally tested for and
448 *Schistosomiasis mansoni* (Kato-Katz). Given the low prevalence of parasitic infections in The
449 Netherlands, Europeans were assumed negative for parasitic infections.

450

451 *Sample collection and PBMC isolation*

452 From the participants selected for the immunology study, venous blood was collected in heparin,
453 EDTA and dry tubes for cell isolation, full blood count (SugarSpin and Senegal only), and serology
454 tests. From each site, peripheral blood mononuclear cells (PBMCs) were isolated from heparinised
455 blood within four hours following blood collection, using standard Ficoll density gradient. The cells
456 were frozen in 20%FCS/10%DMSO/RPMI freezing medium and stored in liquid nitrogen. Freezing
457 medium was supplemented with 100 U/ml penicillin (Gibco), 100 U/ml streptomycin (Sigma-
458 Aldrich), 1 mM pyruvate (Sigma-Aldrich), 2 mM glutamate (Sigma-Aldrich).

459

460 *Mass cytometry*

461 *Mass cytometry antibody staining*

462 Antibody panels were designed to phenotype immune cells *ex vivo*. Details on antibodies used are
463 listed in Table S3. Antibody-metal conjugates were either purchased or conjugated using a total of

464 100µg of purified antibody combined with the Maxpar X8 Antibody Labelling Kit (Fluidigm, San
465 Francisco, CA, USA) according to the manufacturer's protocol V7. The conjugated antibody was
466 stored in 200µl of Antibody Stabilizer PBS (Candor Bioscience GmbH, Wangen, Germany) at 4°C.
467 All antibodies were titrated on PBMC samples.

468

469 On the day of the staining, cryopreserved PBMCs were thawed with 20% FCS/2mM Mg^{2+}/1:10.000
470 benzonase/RPMI medium (SugarSpin and Senegal: 50% FCS/RPMI medium) at 37°C and washed
471 twice with 10% FCS/RPMI medium. For phenotyping, 3×10^6 cells per sample were stained based on
472 the Maxpar Nuclear Antigen Staining Protocol V2 (Fluidigm). First, cells were washed with Maxpar
473 staining buffer and centrifuged for 5 min at 400g (SugarSpin and Senegal: 300g) in 5ml Eppendorf
474 tubes.

475

476 For the Senegal and CapTan study, samples were barcoded and measured in two and seven batches,
477 respectively. In every batch, one aliquot of PBMCs from a reference sample was included to
478 normalize staining between batches, resulting in CN_{within}-normalised data. To barcode the samples,
479 PBMCs were resuspended in 50µl of Maxpar staining buffer, and 50µl of barcode mix targeting β2-
480 microglobulin (B2M) was added to each individual sample in a 6-choose-3 scheme using cadmium
481 $(Cd)_{106}$, Cd_{110}, Cd_{111}, Cd_{112}, Cd_{114}, and Cd_{116}. Samples were incubated for 30 min at room
482 temperature and then washed with 4ml of Maxpar Staining Buffer. Cells were centrifuged for 5 min at
483 400g, and the supernatant was removed, resuspended and combined into 1 tube in Maxpar staining
484 buffer.

485

486 Then, the cells were incubated with 5ml (SugarSpin and Senegal: 1ml) of 500× diluted 500µM Cell-
487 ID Intercalator-103Rh (Fluidigm) in staining buffer at room temperature for 15 min to identify dead
488 cells. After washing with staining buffer, cells were incubated with 20µl (SugarSpin and Senegal:
489 5µl) of Human TruStain FcX Fc receptor blocking solution (BioLegend) and 130µl (SugarSpin and
490 Senegal: 45µl) of staining buffer at room temperature for 5 min (SugarSpin and Senegal: 10 min).

491 Then, 150µl (SugarSpin and Senegal: 50µl) of freshly prepared surface antibody cocktail was added
492 and incubated at room temperature for another 30 min (SugarSpin and Senegal: 45 min).
493 Subsequently, cells were washed twice with staining buffer and fixed with 1.6% PFA in 5ml PBS and
494 incubated for 10 min (CapTan only). Cells were spun 800g for 7 min, supernatant was removed after
495 which cells were fixed and permeabilized using the eBioscience Foxp3/Transcription Factor Staining
496 Buffer Set (eBioscience, cat. 00-5523-00). After cells were incubated with 5ml (SugarSpin and
497 Senegal: 1ml) of the freshly prepared Fix/Perm working solution (prepared according to the
498 manufacturer's instructions) for 45 min, cells were spun and washed twice with 1× permeabilization
499 buffer at 800g for 7 min (SugarSpin and Senegal: 5 min). Next, cells were resuspended in 130µl of 1×
500 permeabilization buffer and incubated for 5 min with Human TruStain FcX Fc receptor blocking
501 solution (CapTan only). Then, 150µl (SugarSpin: 50µl) of the intranuclear antibody cocktail was
502 added and incubated for 30 min at room temperature. Following incubation, cells were washed once
503 with 1× permeabilization buffer and once (SugarSpin and Senegal: twice) with staining buffer before
504 fixation with 1.6% PFA in 5mL PBS and incubated for 10 min (CapTan only). Cells were spun and
505 stained with 5ml (SugarSpin and Senegal: 1ml) of 1000× diluted 125 µM Cell-ID Intercalator-Ir
506 (Fluidigm) in Maxpar Fix and Perm Buffer (Fluidigm) at room temperature for 1h (SugarSpin and
507 Senegal: at 4°C overnight) to stain all cells. After two (SugarSpin and Senegal: three) washes with
508 staining buffer and centrifugation at 800g, cells were resuspended in RPMI 20% FCS 10% DMSO
509 and stored at -80°C until acquisition. For the SugarSpin and Senegal study, cells were stored as a
510 pellet at 4°C and measured within 2 days.
511
512 *Mass cytometry antibody acquisition*
513 For the Senegal and CapTan study, cells were thawed on the day of acquisition in RPMI 50% FCS,
514 spun and washed twice with Maxpar staining buffer. Samples were measured with a Helios mass
515 cytometer (Fluidigm), which was automatically tuned according to Fluidigm's recommendations.
516 Before measuring, cells were counted, washed with Milli-Q water, passed over a cell strainer, and
517 brought to a concentration of 1.0×10^6 cells/ml with 10% EQ Four Element Calibration Beads
518 (Fluidigm) in Milli-Q water. Mass cytometry data were acquired and analyzed on-the-fly using dual-

count mode and noise-reduction on. Next to channels to detect antibodies, channels for intercalators ($_{103}$Rh, $_{191}$Ir, and $_{193}$Ir), calibration beads ($_{140}$Ce, $_{151}$Eu, $_{153}$Eu, $_{165}$Ho, and $_{175}$Lu), and background/contamination ($_{133}$Cs, $_{138}$Ba, and $_{206}$Pb) were acquired. After data acquisition, the mass bead signal was used to normalize the short-term signal fluctuations with the reference EQ passport P13H2302 during the course of each experiment. When applicable, normalized FCS files were concatenated using Helios software without removing the beads.

Data analysis

All data preprocessing and statistics were performed in R v4.2.2 and RStudio Server v2022.03.999. All *p*-values were corrected for multiple testing using to the Benjamini-Hochberg procedure (and referred to as *q*-values). *q*-values < 0.05 were considered statistically significant.

Data preprocessing

First, raw (bead-normalized) data were preprocessed through a unified pipeline. Briefly, the pipeline included automated gating using Gaussian parameters (*CyTOFClean* R-package; v1.03beta; https://github.com/JimboMahoney/cytofclean) and automated quality control for signal stability over acquisition time (*PeacoQC* v1.9.3 R-package (Emmaneel et al., 2022); parameters recommended for mass cytometry data). Next, automatic gating was applied to select for intact/DNA^{+}-($_{191}$Ir and $_{193}$Ir channels), CD45^{+}- ($_{89}$Y), live cells (live/dead staining) (*openCyto* v2.10.1 R-package). All automatically set gates were manually inspected. Samples were compensated (only CapTan study) and debarcoded (CapTan and Senegal studies; *CATALYST* v1.22.0 R-package). Resulting data were converted from .FCS-files into a SingleCellExperiment-object ('raw'). Data were transformed using a hyperbolic arcsinh-transformation with a cofactor of 5 for downstream processing, unless otherwise specified.

Next, reference samples collected from healthy European adults included in each individual batch (CapTan and Senegal studies) were used to train a CytoNorm-model (*CytoNorm* v0.0.17 R-package; CytoNorm.train-function; nQ = 101; goal = 'mean'; *k* = 5). The trained model was applied to all

546 samples, adjusting for batch effects within studies (CN_{within}; CytoNorm.normalize-function). The
547 SugarSpin-study was not acquired in batches and therefore was added to the CN_{within}-dataset without
548 further processing of the 'raw' data.

549

550 *Data integration methods*

551 When merging mass cytometry data, appropriately adjusting for batch effects, within and between
552 studies, is a major challenge. Batch effects stem from differences in sensitivity across cytometers,
553 metal sensitivity and oxidation, variability in antibodies and channel spillover (Rybakowska et al.,
554 2021). These effects can be minimized by using standardized experimental protocols, reducing
555 sources of technical variation. Furthermore, identical technical replicates are typically included to
556 correct variation in marker intensities between batches within studies based on a goal distribution
557 (Van Gassen et al., 2020). However, existing datasets generally lack identical replicates that allow
558 adjustment of batch effects between datasets collected over time.

559 We here assessed four methods to adjust between-study batch effects, including CytofIn (Lo et al.,
560 2022), Harmony (Korsunsky et al., 2019), quantile normalization and CytoNorm (Van Gassen et al.,
561 2020). Two-step normalization approaches were not considered. For CytofIn (Lo et al., 2022) (mode
562 = 'meanshift'; default), the same reference samples as used to generate the CN_{within}-normalized data
563 were used. For the SugarSpin study, one randomly chosen European sample was considered the
564 reference for this study. For quantile and CytoNorm (between studies; $CN_{between}$), *in silico* reference
565 samples were generated by subsampling 1M cells per study, across study groups. Reference samples
566 were inspected using t-SNE visualizations. Next, quantile and CytoNorm were run with similar
567 settings to the CN_{within}-normalization (nQ = 101; goal = 'mean'; k = 5), except that metaclustering
568 performed using the metaClustering_hclust-function. All cells with arcsinh(5)-transformed expression
569 values below zero or above eight were removed.

570

571 *Cell clustering*

572 Study-specific CN_{within}-normalized and integrated $CN_{between}$-normalised datasets were subjected to
573 flowSOM-clustering (15 × 15 hexagonal grid; rlen=100; *kohonen* v3.0.11 R-package), followed by
574 metaclustering at various values of *k* (total number of clusters), using the *ConsensusClusterPlus* v1.62
575 R-package (reps = 100, distance = 'euclidean'). The clustering map was trained on 100k cells per
576 sample, the remaining cells were mapped to the trained map (*predict.kohonen*-function). For choice of
577 the optimal value for *k,* see below.
578
579 *Diversity measures*
580 Immune profile diversity measures (richness, Shannon and Simpson indices) were calculated using
581 the *vegan* R-package v2.6-4. Richness was defined as the number of cluster present at >0.1% of
582 $CD45^{+}$-cells. Statistical significance was assessed using a linear model with group as predictor, while
583 adjusting for study. Estimates and *p*-values for each pairwise comparison between groups (e.g. urban
584 vs rural) were extracted using the *emmeans* v1.8.5 R-package.
585
586 *Automated cell cluster annotations*
587 Cell clusters before (CN_{within}-normalized data) and after ($CN_{between}$-normalised data) were subsequently
588 subjected to an automated cell labeling algorithm. Briefly, for each given marker, the algorithm
589 assesses the distribution of that marker across all cell clusters. Marker distributions are then clustered
590 using hierarchical clustering to define two groups: a 'positive' and a 'negative' group of marker
591 distributions. Subsequently, for each distribution we check how the median expression relates to both
592 the positive and negative groups of distributions. If the median is higher than the 5th percentile of the
593 positive group, the cluster is deemed positive for that marker. If the median is lower than the 95th
594 percentile of the negative group, the cluster is deemed negative for that marker. If neither of these
595 conditions applies, then the marker is considered neutral for that cluster. In this manner we define for
596 each cluster whether a marker is positive, negative or neutral (i.e. not clearly positive or negative). To
597 evaluate the performance of the automated cell labeler, post-integration cell labels were compared to
598 pre-integration labels (considered 'ground truth'). To measure the accuracy of the labelling, the F1
599 score (harmonic mean of the precision and recall) was computed, for every cell population (*yardstick*

600 R-package; f_meas-function; average = ‘binary’). The overall F1 score per dataset were computed as
601 the median of F1 scores across cell populations (excluding populations labeled as ‘missing’ or
602 ‘other’).
603
604 *Dataset-level quantification of data integration*
605 To assess integration, local inverse Simpson index (LISI)-scores were calculated based on 50k cells
606 per study (150k cells total) using default parameters (perplexity = 30; neighbourhood size = 90 cells)
607 (Korsunsky et al., 2019). LISI-scores were calculated to assess whether clusters of cells are well-
608 mixed across studies. If cells are well-mixed, LISI-scores are near the total number of studies in our
609 analysis (i.e. 3). Second, we used *k*-nearest-neighbor batch-effect test (kBET (Buttner et al., 2019)) to
610 quantify batch effects. Briefly, kBET evaluates the accordance a the local fraction of cells in a given
611 batch compared to the global fraction of cells in that batch. Cells are considered well matched if the
612 batch label distribution of local fractions are similar to the global fraction. To estimate label
613 distributions in local fractions, the algorithm creates *k*-nearest neighbour matrix (sample size; 900
614 cells) and choses 10% of the cells to check the batch label distribution in its neighbourhood (with
615 neighborhoodsize *k0*, ranging between 1 to sample size). If the (observed) local batch label
616 distribution in this subset of cells is sufficiently similar to the global batch label distribution, the χ^2-
617 test does not reject the null hypothesis (so all batches are considered well-mixed). The subsampling is
618 performed over 100 repeats for each neighborhood size.
619
620 *Subset-level quantification of data integration*
621 To quantify data integration across larger subsets of cells (i.e. cluster, subset or lineage), we
622 calculated a (global) inverse Simpson index (ISI)-score across all cells belonging to a given subset.
623 Here, ISI-scores differ from LISI-scores, as the latter are calculated across local neighborhood of a set
624 of cells. Despite that, ISI-scores significantly correlated with mean LISI scores for each cluster
625 (Spearman's rank correlation 0.43; p-value = 2.8×10^{-11}), indicating that the global ISI-scores
626 adequately captured local mixing of studies. ISI-scores were calculated across European samples, as

627 these are expected to show no or very limited variation between studies. Therefore, any variation
628 quantified using (L)ISI-scores is likely the result of batch-effect and not biological variation. These
629 scores were compared to ISI-scores based on non-European samples; relatively low scores (arbitrary
630 minimal difference >0.45) in non-Europeans compared to Europeans could indicate population-
631 specific effects in well-integrated cell clusters ($ISI_{EU} > 2.5$).

632

633 *Statistics*

634 PERMANOVA-tests were used to assess the overall effect of study/group on the immune cell
635 frequency data matrix (univariable tests, method = 'euclidean', 9,999 permutations; *vegan* R-package
636 v2.6-4). The statistical significance of the effect of group was assessed with permutations restricted
637 within study strata where appropriate.

638 Principal component analysis (PCA) was performed on cell cluster frequencies of all individuals
639 (*prcomp* R-function). Cell frequencies were centered and scaled to have unit variance.

640 For visualization, cells were embedded in a two dimensional t-distributed Stochastic Neighbor
641 Embedding (t-SNE) map using the FIt-SNE algorithm v1.2.1 (Linderman et al., 2019). FIt-SNE was
642 performed on a downsampled dataset including 50,000 cells per study (max_iter = 1,000; learning rate
643 = *n* cells/12; perplexity = *n* cells/100).

644 To compare the abundance of cell clusters between urban Europeans and rural and urban living non-
645 Europeans we employed a generalized linear mixed model (binomial = 'family'; link = 'logit'; *lme4*
646 R-package v1.1-31). The frequency for each identified lineage, subset or cluster (divided by total
647 $CD45^+$ cells) was considered the dependent variable, 'group' was a fixed explanatory variable and
648 'study ID' and 'sample ID' were included as random intercepts. 'sample ID' was included as random
649 effect to deal with any under- or overdispersion due to the binomial nature of the model. This 'full'
650 model was compared to a 'reduced' model from which 'group' was removed to assess (the
651 significance of) its effect (ANOVA). Resulting *p*-values were corrected for multiple testing
652 (simultaneously accounting for lineage-, subset- and cluster-level analyses). Following, estimates and

p-values for each pairwise comparison between groups (e.g. urban vs rural) were extracted using the *emmeans* v1.8.5 R-package. Statistical significance of these pairwise comparisons was assessed using the Tukey *post hoc* test. To optimize the visualization of differences between groups using boxplots, we performed median absolute deviation (MAD)-filtering, not showing samples with cluster/subset frequencies > 25 × MAD.

Rural-urban classification

As a proof-of-principle, we used a wide range of machine learning models to investigate if we could discriminate urban- from rural-living individuals based solely on cellular immunological signatures. Modeling was performed on subset-level cell frequencies and the 80th percentile of marker intensity values of activation markers (defined as CD152 [CTLA-4], CD161, CD196 [CCR6], CD197 [CCR7], CD278 [ICOS], CD279 [PD1], TBX21 [Tbet] and KLRG1) for each subset, all features were scaled to unit variance. Data was split in a train (70% of the data) and test data partition (*caret* v7.0 R-package), partitioning of data was performed by splitting the studies in equal proportion to minimize bias towards a specific study. Automated model tuning was performed on training data using 5-fold cross-validation over 10 repeats (*caretEnsemble* v4.0.1 R-package). Model performance was compared between the following models: shrinkage discriminant analysis (sda), linear discriminant analysis (lda), elastic-net regularized generalized linear model (glmnet), random forest (ranger), eXtreme gradient boosting (xgbLinear, xgbTree), least squares support vector machine (lssvmRadial), Naïve Bayes (naive_bayes), generalized linear model (glm) and generalized partial least squares (gpls).

Acknowledgements

This study is part of the EDCTP2 program supported by the European Union and by grants from the Dutch Research Organization (NWO) through the Spinoza prize awarded to Maria Yazdanbakhsh, the European Research Council (ERC) via the ERC Advanced Grant 'REVERSE' awarded to Maria

Yazdanbakhsh (Grant No: 101055179), the LUMC Excellent Student Fellowship awarded to Marloes M.A.R. van Dorst and the LUMC Global PhD Fellowship awarded to Jeremia J. Pyuza. We would to like acknowledge all clinical and research staff at study sites in Tanzania, Senegal and Indonesia who helped to make this study possible. We would also like to acknowledge the LUMC core facility for providing mass cytometry services. Finally, we would like to thank all volunteers who participated in this study.

Authors contributions

Conceptualization, K.A.S., W.A.A.d.S.P., M.Y.; Methodology, J.J.P., M.M.A.R.v.D., M.K., Y.C.M.K.; Data Curation, K.A.S., W.A.A.d.S.P.; Formal Analysis, K.A.S., W.A.A.d.S.P., M.M., A.M., M.C., S.P.J.; Investigation, J.J.P., M.M.A.R.v.D., D.LT., T.S., J.P., M.M.; Writing - Original Draft, K.A.S., W.A.A.d.S.P.; Review & Editing, all authors; Supervision, A.M., S.P.J., W.A.A.d.S.P., M.Y.; Funding Acquisition, M.Y. All authors read and approved the final manuscript.

Competing interest

The authors declare that they have no competing interest.

Data and materials availability

All data associated with this study are present and available upon request.

699 **Legends**

700

701 **Figure 1 | CytoNorm successfully integrates three mass cytometry datasets.** A) Geographical map
702 of studies and study sites. Symbols indicate EU, urban or rural sites. B) Graphical representation of
703 sample numbers and the study design. C-D) t-distributed Stochastic Neighbor Embedding (t-SNE)
704 visualizations for each dataset C) pre- ['raw' and CN_{within}] and D) post-integration [CytofIn, Harmony,
705 quantile and $CN_{between}$-normalisation]; *n* = 50k random cells/study); cells are colored according to
706 study (panels) and lineage (zoomed-in area). E) Stacked bar chart of lineage frequencies pre- (CN_{within};
707 'before') and post-integration ($CN_{between}$; 'after') for each of the studies. Each bar section represents
708 the mean frequency of that cell lineage for the corresponding group. F) Local inverse Simpson index
709 (LISI) scores of study across datasets (pre- and post-integration). G) Principal component analysis
710 (PCA) was applied to cell cluster frequencies (centered and scaled to unit variance) of individual
711 samples (*n* = 172). Each participant is reflected as one data point. Data points are colored based on
712 group (European, EU; Rural and Urban). The shape of datapoints indicates the study (CapTan,
713 Tanzania; Senegal and SugarSpin, Indonesia studies). Ellipses reflect the data spread at a level of
714 confidence of 68% (one standard deviation in a normal distribution).

715

716 **Figure 2 | Automated post-integration subset-level annotations of cellular immune profiles**
717 **adequately capture cellular immune profiles.**

718 A) Confusion matrices for each study, showing the subset-level annotations generated by the
719 automatic labelling algorithm before and after data integration. Colours and values in the cells reflect
720 how a given pre-integration label is distributed across post-integration labels ('fraction'). B) Stacked
721 bar plot showing cell frequencies (number of cells/total $CD45^+$ cells) for each subset. Subset labels
722 were based on automatic cell labelling before (CN_{within}) and after ($CN_{between}$) data integration. Cell
723 frequencies before [striped] and after [filled] integration are shown and facetted according to cell
724 lineage. C) F1 scores (harmonic mean of the precision and recall) as a measure of labelling accuracy

725 was computed for each cell subset (comparing data before [truth] and after [prediction] integration).
726 D) Alluvial diagram showing the results of which subsets were re-labeled after the automatic cell
727 labeler.

728

729 **Figure 3 | Differential cell frequencies between urban and rural-living individuals.**

730 A) and B) Venn diagrams indicating the number cell clusters that show differences in cell frequencies
731 between 1) rural and urban-living non-Europeans, 2) rural-living individuals and Europeans and 3)
732 urban-living non-Europeans and Europeans. Colors indicate the direction of the EU-urban-rural-
733 gradient: A) blue, positively associated with rural-lifestyle; B) orange, negatively associated with
734 rural-lifestyle. The strength of the EU-urban-rural-gradient was based on the number and
735 directionality of significant pairwise comparisons (Tukey-adjusted p-value < 0.05; see schematic right
736 of each Venn diagram). Significance for all comparisons was considered strongest evidence of a true
737 rural-urban gradient (full; 1., 2. and 3.), followed by 1. and 2. or 2. and 3. (partial), and only urban-
738 compared to rural-living individuals (Ru-Ur/limited; 1.). Significance of 2. and 3. (i.e. not 1.) was
739 suggestive of European compared to non-European differences, rather than evidence for a rural-urban
740 gradient and these comparisons were therefore not further considered (grey). C) Volcano plot showing
741 differential frequency results at subset and cell cluster level. Statistical significance of pairwise
742 comparisons was derived from a linear mixed model with cell frequency as outcome, group
743 (EU/rural/urban) as fixed effect and sample ID and study ID as random effects. Model estimates and
744 corresponding -$\log_{10}$-transformed Tukey-adjusted p-values for rural- compared to urban-living
745 individuals were extracted using the *emmeans* R-package. Analyses were performed on n = 172
746 individuals. Each point represents a subset/cell cluster, subsets/clusters with p_{Tukey}-values<0.05 are
747 colored by cell lineage and labelled with subset name/cluster ID. D) Box plots showing cell
748 frequencies for a representative selection of cell clusters (10 out of in total 20; focusing on those
749 clusters showing a full or partial EU-rural-urban gradient; remaining clusters shown in Figure S7).
750 Boxplots represent the 25th and 75th percentiles (lower and upper boundaries boxes, respectively), the
751 median (middle horizontal line), and measurements that fall within 1.5 times the interquartile range

752 (IQR; distance between 25th and 75th percentiles; whiskers). Directly right of the each boxplot,
753 individual data points are shown. The shape and dodge of the data points corresponds with the study
754 the samples originated from. Statistical significance of pairwise comparisons was derived from a
755 linear mixed model with cell frequency as outcome, group (EU/rural/urban) as fixed effect and sample
756 ID and study ID as random effects. Tukey-adjusted *p*-values for pairwise comparisons between
757 Europeans, non-European rural- and urban-living individuals were extracted using the *emmeans* R-
758 package. For each panel, the BH-adjusted $ANOVA_{FDR}$-value of the differences across Europeans,
759 non-European urban- and rural-living individuals is shown. The inverse Simpson Index in European
760 samples (ISI_{EU}) is also depicted, where higher ISI_{EU} scores indicate better integrated cell clusters. Text
761 colour corresponds with the colors in the Venn diagrams in A). Asterisks denote statistical
762 significance (*, $p_{Tukey} \leq 0.05$; **, $p_{Tukey} \leq 0.01$; ***, $p_{Tukey} \leq 0.001$). E) ISI_{EU} compared to $ISI_{non\text{-}EU}$
763 scores. $ISI_{non\text{-}EU}$ scores that were substantially lower (defined as >0.45 difference) compared to ISI_{EU}
764 scores were considered possible population-specific cell clusters (only considering well integrated
765 clusters with ISI_{EU} >2.5).

766

767 **Figure 4 | Classification models based on immune signatures are able to discriminate urban-**
768 **and rural-living individuals.**

769 A) Boxplots depicting the model accuracy on the training data. All models were trained ten times with
770 resampled train data. Dots below the respective boxplots represent the accuracy based on the test data.
771 The black square represents the accuracy on the complete test data and colored dots indicate the study,
772 red, yellow and green, respectively, for CapTan, Senegal and Sugarspin. Boxplots represent the 25th
773 and 75th percentiles (lower and upper boundaries boxes, respectively), the median (middle horizontal
774 line), and measurements that fall within 1.5 times the interquartile range (IQR; distance between 25th
775 and 75th percentiles; whiskers). B) Boxplots of the sixteen highest contributing parameters obtained
776 from the best performing model (glmnet).

777

Supplementary figures

Figure S1 | Data preprocessing and integration pipeline. Flowchart showing the data preprocessing, quality control and integration methods applied.

Figure S2 | kBET mean rejection rates depend by neighborhood size. The dashed vertical lines indicate the optimal neighborhood size for batch-effect detection, that is, where the rejection rate is maximal. Shaded areas represent the 95th percentile of n = 100 repeated kBET runs. In each run, the number of tested neighborhoods was 10% of the sample size (i.e., 90 cells).

Figure S3 | Integration metrics to assess clustering depth.

A) Median inverse Simpson index (within European samples; study) across all cell subsets (clusters, codes, subsets or lineages). Higher values indicate higher diversity of study-labels within a given group of cells, suggesting better integration. The optimal number of clusters was k = 125 (first local peak in median ISI across clusters with $k \geq 100$). B) Boxplots of inverse Simpson indices (within European samples; study) for cell clusters (for a selection of k-values), codes, subsets and lineages. Boxplots represent the 25th and 75th percentiles (lower and upper boundaries boxes, respectively), the median (middle horizontal line), and measurements that fall within 1.5 times the interquartile range (IQR; distance between 25th and 75th percentiles; whiskers). C) and D) Stacked bar plots showing inverse Simpson index categories, indicating low ($\leq$ 2.2), moderate (2.2 – 2.5), high (2.5-2.8) and very high (>2.8) indices. Percentages were calculated by dividing the number of cell subsets (i.e. cell clusters, codes, subsets or lineages) within a given inverse Simpson index category by the total number of cell subsets (C). In D) we additionally normalized for the number of cells within each cell subset. Here, a considerable drop in the percentage of cells allocated to a cell cluster with ISI-score >2.8 can be appreciated.

803

804 **Figure S4 | Heatmap showing median marker expression for each cluster.** Clusters were based on
805 SOM and hierarchical clustering. Each tile depicts the median expression of a given marker (rows) for
806 a specific cluster (columns). The heatmap is stratified based on cell lineage.

807

808 **Figure S5 | Highest cell cluster diversity in rural-living individuals compared to urban-living**
809 **and European individuals.** Richness (number of cell clusters present at >0.1% of $CD45^+$-cells),
810 Shannon and Simpson diversity measures by A) group and B) group, stratified by lineage ($CD4^+$ or
811 $CD8^+$ T cells). Diversity measures were calculated based on rarefied data, subsampling each sample to
812 a 'depth' of 70,000 cells. Boxplots represent the 25th and 75th percentiles (lower and upper
813 boundaries of boxes, respectively), the median (middle horizontal line), and measurements that fall
814 within 1.5 times the interquartile range (IQR; distance between 25th and 75th percentiles; whiskers).
815 Statistical significance was assessed using linear models with group and study as fixed effects.
816 Statistical significance of differences between each group was assessed using the *emmeans()*-function.
817 P-values were corrected for multiple testing using the Benjamini-Hochberg method. Asterisks denote
818 statistical significance (*, $q \leq 0.05$; **, $q \leq 0.01$; ***, $q \leq 0.001$).

819

820 **Figure S6 | Subset frequencies between Europeans, rural- and urban-living individuals.** Box
821 plots showing subset frequencies (all detected subsets shown). Boxplots represent the 25th and 75th
822 percentiles (lower and upper boundaries boxes, respectively), the median (middle horizontal line), and
823 measurements that fall within 1.5 times the interquartile range (IQR; distance between 25th and 75th
824 percentiles; whiskers). Directly right of the each boxplot, individual data points are shown. The shape
825 and dodge of the data points corresponds with the study the samples originated from. Statistical
826 significance of pairwise comparisons was derived from a linear mixed model with cell frequency as
827 outcome, group (EU/rural/urban) as fixed effect and sample ID and study ID as random effects.
828 Tukey-adjusted *p*-values for pairwise comparisons between Europeans, non-European rural- and

829 urban-living individuals were extracted using the *emmeans* R-package. For each panel, the BH-
830 adjusted $ANOVA_{FDR}$-value of the differences across Europeans, non-European urban- and rural-living
831 individuals is shown. The inverse Simpson Index in European samples (ISI_{EU}) is also depicted, where
832 higher ISI_{EU} scores indicate better integrated subsets. Analyses were performed on $n = 172$
833 individuals. Asterisks denote statistical significance (*, $p_{Tukey} \leq 0.05$; **, $p_{Tukey} \leq 0.01$; ***, $p_{Tukey} \leq$
834 0.001).

835

836 **Figure S7 | Differential cell frequencies between rural- and urban-living individuals.** Boxplots
837 showing cell frequencies for cell clusters showing significant differences between rural- and urban-
838 living individuals (remaining 10/20 clusters; 10/20 depicted in Figure 3D; p_{Tukey}-value<0.05 for at
839 least one comparison; see legend Figure 3D).

840

841 **Figure S8 | Th2 cell marker expression.** A-C) t-distributed Stochastic Neighbor Embedding (t-SNE)
842 visualization Th2 cells (clusters 57 and 58; n = 1k random cells/subject). A) Global location of
843 $CD161^+$ and $GATA^+$ Th2 cells. B) t-SNE embeddings were colored according to marker expression of
844 CD294 (CRTH2), GATA3, CD161, KLRG1 (MAFA) and CD297 (PD-1) C) cluster allocation (based
845 on global clustering across all cells). D) Density features of Th2 cells. E) Distribution of marker
846 expression of CD294 (CRTH2), GATA3, CD161, KLRG1 (MAFA) and CD297 (PD-1) for each Th2
847 cluster (57 and 58). Area under the ridges was colored according to marker expression quartile.

848

849 **Figure S9 | Lower rates of naïve CD8+ T cells in rural-living non-Europeans.** A-B and D) t-
850 distributed Stochastic Neighbor Embedding (t-SNE) visualization $CD8^+$ T cells (based on cluster
851 annotation; n = 26 clusters; n = 1k random cells/subject). A) Global location of $CD8^+$ naïve, effector
852 memory (EM), effector memory T cells that re-express CD45RA (EMRA), $CD161^+$ EM, and central
853 memory (CM) cells. B) t-SNE colored according to cluster allocation (based on global clustering
854 across all cells). D) t-SNE colored according to marker expression of CD45RA, CD45RO, CD197

855 (CCR7), CD127 (IL-7RA), CD161, KLRGI (MAFA), CD279 (PD-1), Tbet and HLA-DR. C) Density
856 features of $CD8^+$ T cells. E) Distribution of marker expression of CD279 (PD-1), KLRG1 (MAFA),
857 Tbet, CD161 and HLA-DR for each $CD8^+$ T cell cluster. Area under the ridges was colored according
858 to marker expression quartile.

859

860 **Figure S10 | Differential cell frequencies of well-integrated, study-specific cell clusters.** Box plots
861 showing cell cluster frequencies showing significant differences between studies, stratified between
862 non-Europeans (non-EU) and Europeans (EU). The selection of these clusters was based on Figure
863 3E. Boxplots represent the 25th and 75th percentiles (lower and upper boundaries boxes, respectively),
864 the median (middle horizontal line), and measurements that fall within 1.5 times the interquartile
865 range (IQR; distance between 25th and 75th percentiles; whiskers). Directly right of the each boxplot,
866 individual data points are shown. The shape and dodge of the data points corresponds with the study
867 the samples originated from. Statistical significance of pairwise comparisons was derived from a
868 linear mixed model with cell frequency as outcome, group (EU/rural/urban) as fixed effect and sample
869 ID and study ID as random effects. Tukey-adjusted *p*-values for pairwise comparisons between
870 Europeans, non-European rural- and urban-living individuals were extracted using the *emmeans* R-
871 package. For each panel, the BH-adjusted $ANOVA_{FDR}$-value of the differences across Europeans,
872 non-European urban- and rural-living individuals is shown. The inverse Simpson Index in European
873 samples (ISI_{EU}) is also depicted, where higher ISI_{EU} scores indicate better integrated cell clusters.
874 Analyses were performed on $n = 172$ individuals. Asterisks denote statistical significance (*, $p_{Tukey} \leq$
875 0.05; **, $p_{Tukey} \leq 0.01$; ***, $p_{Tukey} \leq 0.001$).

876

877

878 **Supplementary tables**

879 **Table S1 | Dataset metadata.** Dataset metadata for CapTan, Senegal and SugarSpin studies.

880

881 **Table S2 | Baseline characteristics across study groups.** EU, European; Urban, urban-living non-
882 Europeans; Rural, rural-living non-Europeans. n (%) (categorical variables) or median (IQR)
883 (continuous variables) shown, [a] Kruskal-Wallis rank sum test; [b] Pearson's Chi-squared test.

884

885 **Table S3 | Mass cytometry antibody panel.** CCR, C-C chemokine receptor. CD, cluster
886 of differentiation. CRTH2, prostaglandin D2 receptor 2. CXCR, CXC chemokine receptor. HLA-DR,
887 human leukocyte antigen-D-related. IL-2R, interleukin-2 receptor. IL-7Rα, interleukin-7 receptor α.
888 KLRG1, killer cell lectin-like receptor subfamily G member 1. MAFA, mast cell function-
889 associated antigen. PD- 1, programmed cell death protein 1. TCR, T cell receptor. RORγt, related
890 orphan receptor gamma t.

891

892 **Table S4 | 'Rules' automated cell labeller.** For each lineage and subset, positive (pos), negative
893 (neg), not positive (i.e. negative/neutral; not_pos), not negative (i.e. positive/neutral; not_neg)
894 markers are shown. For each cell cluster, markers were classified as 'positive', 'negative' or 'neutral'
895 by comparing marker intensity distribution of that cluster to the marker intensity distribution in all
896 other cell clusters.

897

898 **Table S5 | Cell annotations.** Annotation of each cluster separated on lineage, subset and cluster level.
899 Both the annotation of the automatic cell labeller and the revised annotation is included (manual).

900

901

902 **References**

903 Abdelaal, T., van Unen, V., Höllt, T., Koning, F., Reinders, M. J. T., & Mahfouz, A. (2019). Predicting
904 Cell Populations in Single Cell Mass Cytometry Data. *Cytometry A*, *95*(7), 769-781.
905 https://doi.org/10.1002/cyto.a.23738
906 Brodin, P., & Davis, M. M. (2017). Human immune system variation. *Nat Rev Immunol*, *17*(1), 21-29.
907 https://doi.org/10.1038/nri.2016.125
908 Brodin, P., Jojic, V., Gao, T., Bhattacharya, S., Angel, C. J., Furman, D., Shen-Orr, S., Dekker, C. L.,
909 Swan, G. E., Butte, A. J., Maecker, H. T., & Davis, M. M. (2015). Variation in the human
910 immune system is largely driven by non-heritable influences. *Cell*, *160*(1-2), 37-47.
911 https://doi.org/10.1016/j.cell.2014.12.020
912 Buttner, M., Miao, Z., Wolf, F. A., Teichmann, S. A., & Theis, F. J. (2019). A test metric for assessing
913 single-cell RNA-seq batch correction. *Nat Methods*, *16*(1), 43-49.
914 https://doi.org/10.1038/s41592-018-0254-1
915 de Jong, S. E., van Unen, V., Manurung, M. D., Stam, K. A., Goeman, J. J., Jochems, S. P., Hollt, T.,
916 Pezzotti, N., Mouwenda, Y. D., Betouke Ongwe, M. E., Lorenz, F. R., Kruize, Y. C. M., Azimi, S.,
917 Konig, M. H., Vilanova, A., Eisemann, E., Lelieveldt, B. P. F., Roestenberg, M., Sim, B. K. L., . . .
918 Yazdanbakhsh, M. (2021). Systems analysis and controlled malaria infection in Europeans
919 and Africans elucidate naturally acquired immunity. *Nat Immunol*, *22*(5), 654-665.
920 https://doi.org/10.1038/s41590-021-00911-7
921 de Ruiter, K., Jochems, S. P., Tahapary, D. L., Stam, K. A., Konig, M., van Unen, V., Laban, S., Hollt, T.,
922 Mbow, M., Lelieveldt, B. P. F., Koning, F., Sartono, E., Smit, J. W. A., Supali, T., &
923 Yazdanbakhsh, M. (2020). Helminth infections drive heterogeneity in human type 2 and
924 regulatory cells. *Sci Transl Med*, *12*(524). https://doi.org/10.1126/scitranslmed.aaw3703
925 Duurland, C. L., Santegoets, S. J., Abdulrahman, Z., Loof, N. M., Sturm, G., Wesselink, T. H., Arens, R.,
926 Boekestijn, S., Ehsan, I., van Poelgeest, M. I. E., Finotello, F., Hackl, H., Trajanoski, Z., Ten
927 Dijke, P., Braud, V. M., Welters, M. J. P., & van der Burg, S. H. (2022). CD161 expression and
928 regulation defines rapidly responding effector CD4+ T cells associated with improved survival
929 in HPV16-associated tumors. *J Immunother Cancer*, *10*(1). https://doi.org/10.1136/jitc-2021-
930 003995
931 Emmaneel, A., Quintelier, K., Sichien, D., Rybakowska, P., Maranon, C., Alarcon-Riquelme, M. E., Van
932 Isterdael, G., Van Gassen, S., & Saeys, Y. (2022). PeacoQC: Peak-based selection of high
933 quality cytometry data. *Cytometry A*, *101*(4), 325-338. https://doi.org/10.1002/cyto.a.24501
934 Epstein, J. E., Paolino, K. M., Richie, T. L., Sedegah, M., Singer, A., Ruben, A. J., Chakravarty, S.,
935 Stafford, A., Ruck, R. C., Eappen, A. G., Li, T., Billingsley, P. F., Manoj, A., Silva, J. C., Moser, K.,
936 Nielsen, R., Tosh, D., Cicatelli, S., Ganeshan, H., . . . Hoffman, S. L. (2017). Protection against
937 Plasmodium falciparum malaria by PfSPZ Vaccine. *JCI Insight*, *2*(1), e89154.
938 https://doi.org/10.1172/jci.insight.89154
939 Forconi, C. S., Oduor, C. I., Oluoch, P. O., Ong'echa, J. M., Münz, C., Bailey, J. A., & Moormann, A. M.
940 (2020). A New Hope for CD56(neg)CD16(pos) NK Cells as Unconventional Cytotoxic
941 Mediators: An Adaptation to Chronic Diseases. *Front Cell Infect Microbiol*, *10*, 162.
942 https://doi.org/10.3389/fcimb.2020.00162
943 Fourati, S., Tomalin, L. E., Mule, M. P., Chawla, D. G., Gerritsen, B., Rychkov, D., Henrich, E., Miller, H.
944 E. R., Hagan, T., Diray-Arce, J., Dunn, P., Human Immunology Project, C., Levy, O., Gottardo,
945 R., Sarwal, M. M., Tsang, J. S., Suarez-Farinas, M., Pulendran, B., Kleinstein, S. H., & Sekaly, R.
946 P. (2022). Pan-vaccine analysis reveals innate immune endotypes predictive of antibody
947 responses to vaccination. *Nat Immunol*, *23*(12), 1777-1787. https://doi.org/10.1038/s41590-
948 022-01329-5
949 Gazzinelli-Guimaraes, P. H., Dulek, B., Swanson, P., Lack, J., Roederer, M., & Nutman, T. B. (2024).
950 Single-cell molecular signature of pathogenic T helper subsets in type 2-associated disorders
951 in humans. *JCI Insight*, *9*(7). https://doi.org/10.1172/jci.insight.177720

Godfrey, D. I., Koay, H. F., McCluskey, J., & Gherardin, N. A. (2019). The biology and functional importance of MAIT cells. *Nat Immunol*, *20*(9), 1110-1128. https://doi.org/10.1038/s41590-019-0444-8

Hagan, T., Gerritsen, B., Tomalin, L. E., Fourati, S., Mule, M. P., Chawla, D. G., Rychkov, D., Henrich, E., Miller, H. E. R., Diray-Arce, J., Dunn, P., Lee, A., Human Immunology Project, C., Levy, O., Gottardo, R., Sarwal, M. M., Tsang, J. S., Suarez-Farinas, M., Sekaly, R. P., . . . Pulendran, B. (2022). Transcriptional atlas of the human immune response to 13 vaccines reveals a common predictor of vaccine-induced antibody responses. *Nat Immunol*, *23*(12), 1788-1798. https://doi.org/10.1038/s41590-022-01328-6

HIPC-CHI Signatures Project Team, & HIPC-I Consortium. (2017). Multicohort analysis reveals baseline transcriptional predictors of influenza vaccination responses. *Sci Immunol*, *2*(14). https://doi.org/10.1126/sciimmunol.aal4656

Ito, T., Carson, W. F. t., Cavassani, K. A., Connett, J. M., & Kunkel, S. L. (2011). CCR6 as a mediator of immunity in the lung and gut. *Exp Cell Res*, *317*(5), 613-619. https://doi.org/10.1016/j.yexcr.2010.12.018

Korsunsky, I., Millard, N., Fan, J., Slowikowski, K., Zhang, F., Wei, K., Baglaenko, Y., Brenner, M., Loh, P. R., & Raychaudhuri, S. (2019). Fast, sensitive and accurate integration of single-cell data with Harmony. *Nat Methods*, *16*(12), 1289-1296. https://doi.org/10.1038/s41592-019-0619-0

Kotliarov, Y., Sparks, R., Martins, A. J., Mule, M. P., Lu, Y., Goswami, M., Kardava, L., Banchereau, R., Pascual, V., Biancotto, A., Chen, J., Schwartzberg, P. L., Bansal, N., Liu, C. C., Cheung, F., Moir, S., & Tsang, J. S. (2020). Broad immune activation underlies shared set point signatures for vaccine responsiveness in healthy individuals and disease activity in patients with lupus. *Nat Med*, *26*(4), 618-629. https://doi.org/10.1038/s41591-020-0769-8

Li, X., Mukandavire, C., Cucunuba, Z. M., Echeverria Londono, S., Abbas, K., Clapham, H. E., Jit, M., Johnson, H. L., Papadopoulos, T., Vynnycky, E., Brisson, M., Carter, E. D., Clark, A., de Villiers, M. J., Eilertson, K., Ferrari, M. J., Gamkrelidze, I., Gaythorpe, K. A. M., Grassly, N. C., . . . Vaccine Impact Modelling, C. (2021). Estimating the health impact of vaccination against ten pathogens in 98 low-income and middle-income countries from 2000 to 2030: a modelling study. *Lancet*, *397*(10272), 398-408. https://doi.org/10.1016/S0140-6736(20)32657-X

Li, Y. Y., Zhou, L. W., Qian, F. C., Fang, Q. L., Yu, Z. M., Cui, T., Dong, F. J., Cai, F. H., Yu, T. T., Li, L. D., Wang, Q. Y., Zhu, Y. B., Tang, H. F., Hu, B. Y., & Li, C. Q. (2025). scImmOmics: a manually curated resource of single-cell multi-omics immune data. *Nucleic Acids Res*, *53*(D1), D1162-d1172. https://doi.org/10.1093/nar/gkae985

Linderman, G. C., Rachh, M., Hoskins, J. G., Steinerberger, S., & Kluger, Y. (2019). Fast interpolation-based t-SNE for improved visualization of single-cell RNA-seq data. *Nat Methods*, *16*(3), 243-245. https://doi.org/10.1038/s41592-018-0308-4

Lo, Y. C., Keyes, T. J., Jager, A., Sarno, J., Domizi, P., Majeti, R., Sakamoto, K. M., Lacayo, N., Mullighan, C. G., Waters, J., Sahaf, B., Bendall, S. C., & Davis, K. L. (2022). CytofIn enables integrated analysis of public mass cytometry datasets using generalized anchors. *Nat Commun*, *13*(1), 934. https://doi.org/10.1038/s41467-022-28484-5

Luecken, M. D., Buttner, M., Chaichoompu, K., Danese, A., Interlandi, M., Mueller, M. F., Strobl, D. C., Zappia, L., Dugas, M., Colome-Tatche, M., & Theis, F. J. (2022). Benchmarking atlas-level data integration in single-cell genomics. *Nat Methods*, *19*(1), 41-50. https://doi.org/10.1038/s41592-021-01336-8

Manurung, M. D., Heieis, G. A., König, M., Azimi, S., Ndao, M., Veldhuizen, T., Hoving, D., Hoekstra, P. T., Kruize, Y. C. M., Wammes, L. J., Menafra, R., Cisse, M., Mboup, S., Dieye, A., Kloet, S., Tahapary, D. L., Supali, T., Wuhrer, M., Hokke, C. H., . . . Mbow, M. (2025). Systems analysis unravels a common rural-urban gradient in immunological profile, function, and metabolic dependencies. *Sci Adv*, *11*(18), eadu0419. https://doi.org/10.1126/sciadv.adu0419

1002 Mazzucchelli, R., & Durum, S. K. (2007). Interleukin-7 receptor expression: intelligent design. *Nat Rev*
1003 *Immunol*, *7*(2), 144-154. https://doi.org/10.1038/nri2023
1004 Mbow, M., de Jong, S. E., Meurs, L., Mboup, S., Dieye, T. N., Polman, K., & Yazdanbakhsh, M. (2014).
1005 Changes in immunological profile as a function of urbanization and lifestyle. *Immunology*,
1006 *143*(4), 569-577. https://doi.org/10.1111/imm.12335
1007 Mitson-Salazar, A., Yin, Y., Wansley, D. L., Young, M., Bolan, H., Arceo, S., Ho, N., Koh, C., Milner, J.
1008 D., Stone, K. D., Wank, S. A., & Prussin, C. (2016). Hematopoietic prostaglandin D synthase
1009 defines a proeosinophilic pathogenic effector human T(H)2 cell subpopulation with
1010 enhanced function. *J Allergy Clin Immunol*, *137*(3), 907-918.e909.
1011 https://doi.org/10.1016/j.jaci.2015.08.007
1012 Muyanja, E., Ssemaganda, A., Ngauv, P., Cubas, R., Perrin, H., Srinivasan, D., Canderan, G., Lawson,
1013 B., Kopycinski, J., Graham, A. S., Rowe, D. K., Smith, M. J., Isern, S., Michael, S., Silvestri, G.,
1014 Vanderford, T. H., Castro, E., Pantaleo, G., Singer, J., . . . Gaucher, D. (2014). Immune
1015 activation alters cellular and humoral responses to yellow fever 17D vaccine. *J Clin Invest*,
1016 *124*(7), 3147-3158. https://doi.org/10.1172/JCI75429
1017 Natukunda, A., Nkurunungi, G., Zirimenya, L., Nassuuna, J., Zziwa, C., Ninsiima, C., Tumusiime, J.,
1018 Nyanzi, R., Namutebi, M., Kiwudhu, F., van Dam, G. J., Corstjens, P., Kizindo, R., Nkangi, R.,
1019 Kabagenyi, J., Nassanga, B., Cose, S., Wajja, A., Kaleebu, P., . . . Webb, E. L. (2024).
1020 Schistosome and malaria exposure and urban-rural differences in vaccine responses in
1021 Uganda: a causal mediation analysis using data from three linked randomised controlled
1022 trials. *Lancet Glob Health*, *12*(11), e1860-e1870. https://doi.org/10.1016/s2214-
1023 109x(24)00340-1
1024 Pyuza, J. J., van Dorst, M., Barnett, D., Stam, K., Manurung, M., Wammes, L., König, M., Kruize, Y.,
1025 Andongolile, N., Ngowi, A., Shao, E. R., Kullaya, V. I., Mremi, A., Hogendoorn, P. C. W.,
1026 Msuya, S. E., Jochems, S. P., Penders, J., Yazdanbakhsh, M., & de Steenhuijsen Piters, W. A.
1027 A. (2025). Tanzanian gut microbiota profiles linked to high but rapidly waning yellow fever
1028 antibody titers. *NPJ Biofilms Microbiomes*, *11*(1), 110. https://doi.org/10.1038/s41522-025-
1029 00687-w
1030 Pyuza, J. J., van Dorst, M., Stam, K., Wammes, L., König, M., Kullaya, V. I., Kruize, Y., Huisman, W.,
1031 Andongolile, N., Ngowi, A., Shao, E. R., Mremi, A., Hogendoorn, P. C. W., Msuya, S. E.,
1032 Jochems, S. P., de Steenhuijsen Piters, W. A. A., & Yazdanbakhsh, M. (2024). Lifestyle score is
1033 associated with cellular immune profiles in healthy Tanzanian adults. *Brain Behav Immun*
1034 *Health*, *41*, 100863. https://doi.org/10.1016/j.bbih.2024.100863
1035 Rybakowska, P., Van Gassen, S., Quintelier, K., Saeys, Y., Alarcon-Riquelme, M. E., & Maranon, C.
1036 (2021). Data processing workflow for large-scale immune monitoring studies by mass
1037 cytometry. *Comput Struct Biotechnol J*, *19*, 3160-3175.
1038 https://doi.org/10.1016/j.csbj.2021.05.032
1039 Sissoko, M. S., Healy, S. A., Katile, A., Omaswa, F., Zaidi, I., Gabriel, E. E., Kamate, B., Samake, Y.,
1040 Guindo, M. A., Dolo, A., Niangaly, A., Niare, K., Zeguime, A., Sissoko, K., Diallo, H., Thera, I.,
1041 Ding, K., Fay, M. P., O'Connell, E. M., . . . Duffy, P. E. (2017). Safety and efficacy of PfSPZ
1042 Vaccine against Plasmodium falciparum via direct venous inoculation in healthy malaria-
1043 exposed adults in Mali: a randomised, double-blind phase 1 trial. *Lancet Infect Dis*, *17*(5),
1044 498-509. https://doi.org/10.1016/S1473-3099(17)30104-4
1045 Strazar, M., Temba, G. S., Vlamakis, H., Kullaya, V. I., Lyamuya, F., Mmbaga, B. T., Joosten, L. A. B.,
1046 van der Ven, A., Netea, M. G., de Mast, Q., & Xavier, R. J. (2021). Gut microbiome-mediated
1047 metabolism effects on immunity in rural and urban African populations. *Nat Commun*, *12*(1),
1048 4845. https://doi.org/10.1038/s41467-021-25213-2
1049 Tahapary, D. L., de Ruiter, K., Martin, I., van Lieshout, L., Guigas, B., Soewondo, P., Djuardi, Y., Wiria,
1050 A. E., Mayboroda, O. A., Houwing-Duistermaat, J. J., Tasman, H., Sartono, E., Yazdanbakhsh,
1051 M., Smit, J. W., & Supali, T. (2015). Helminth infections and type 2 diabetes: a cluster-

1052 randomized placebo controlled SUGARSPIN trial in Nangapanda, Flores, Indonesia. *BMC*
1053 *Infect Dis*, *15*, 133. https://doi.org/10.1186/s12879-015-0873-4
1054 Temba, G. S., Kullaya, V., Pecht, T., Mmbaga, B. T., Aschenbrenner, A. C., Ulas, T., Kibiki, G., Lyamuya,
1055 F., Boahen, C. K., Kumar, V., Joosten, L. A. B., Schultze, J. L., van der Ven, A. J., Netea, M. G.,
1056 & de Mast, Q. (2021). Urban living in healthy Tanzanians is associated with an inflammatory
1057 status driven by dietary and metabolic changes. *Nat Immunol*, *22*(3), 287-300.
1058 https://doi.org/10.1038/s41590-021-00867-8
1059 Tsang, J. S., Schwartzberg, P. L., Kotliarov, Y., Biancotto, A., Xie, Z., Germain, R. N., Wang, E., Olnes,
1060 M. J., Narayanan, M., Golding, H., Moir, S., Dickler, H. B., Perl, S., Cheung, F., Baylor, H. C., &
1061 Consortium, C. H. I. (2014). Global analyses of human immune variation reveal baseline
1062 predictors of postvaccination responses. *Cell*, *157*(2), 499-513.
1063 https://doi.org/10.1016/j.cell.2014.03.031
1064 van Dorst, M., Pyuza, J. J., Nkurunungi, G., Kullaya, V. I., Smits, H. H., Hogendoorn, P. C. W.,
1065 Wammes, L. J., Everts, B., Elliott, A. M., Jochems, S. P., & Yazdanbakhsh, M. (2024).
1066 Immunological factors linked to geographical variation in vaccine responses. *Nat Rev*
1067 *Immunol*, *24*(4), 250-263. https://doi.org/10.1038/s41577-023-00941-2
1068 Van Gassen, S., Gaudilliere, B., Angst, M. S., Saeys, Y., & Aghaeepour, N. (2020). CytoNorm: A
1069 Normalization Algorithm for Cytometry Data. *Cytometry A*, *97*(3), 268-278.
1070 https://doi.org/10.1002/cyto.a.23904

1071

Figure 1

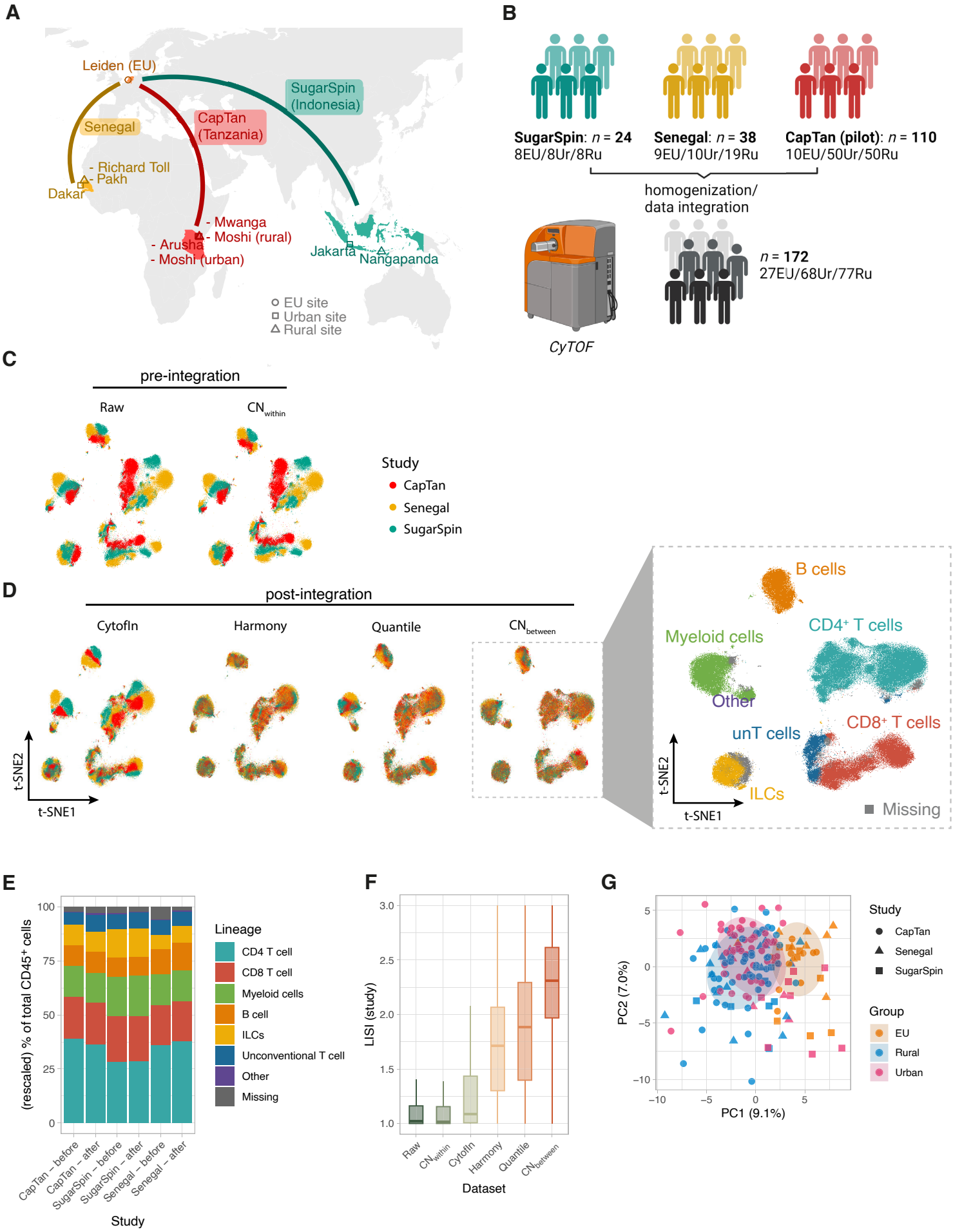
A
Leiden (EU)
SugarSpin (Indonesia)
Senegal
CapTan (Tanzania)
- Richard Toll
- Pakh
Dakar
- Mwanga
- Moshi (rural)
- Arusha
- Moshi (urban)
Jakarta
Nangapanda
EU site
Urban site
Rural site
B
SugarSpin: n = 24
8EU/8Ur/8Ru
Senegal: n = 38
9EU/10Ur/19Ru
CapTan (pilot): n = 110
10EU/50Ur/50Ru
homogenization/
data integration
CyTOF
n = 172
27EU/68Ur/77Ru
C
pre-integration
Raw
CN within
Study
CapTan
Senegal
SugarSpin
D
post-integration
CytoIn
Harmony
Quantile
CN between
t-SNE2
t-SNE1
B cells
CD4+ T cells
Myeloid cells
Other
unT cells
CD8+ T cells
ILCs
Missing
E
(rescaled) % of total CD45+ cells
Lineage
CD4 T cell
CD8 T cell
Myeloid cells
B cell
ILCs
Unconventional T cell
Other
Missing
CapTan – before
CapTan – after
SugarSpin – before
SugarSpin – after
Senegal – before
Senegal – after
Study
F
LISI (study)
Raw
CN within
CytoIn
Harmony
Quantile
CN between
Dataset
G
PC2 (7.0%)
PC1 (9.1%)
Study
CapTan
Senegal
SugarSpin
Group
EU
Rural
Urban

Figure 2

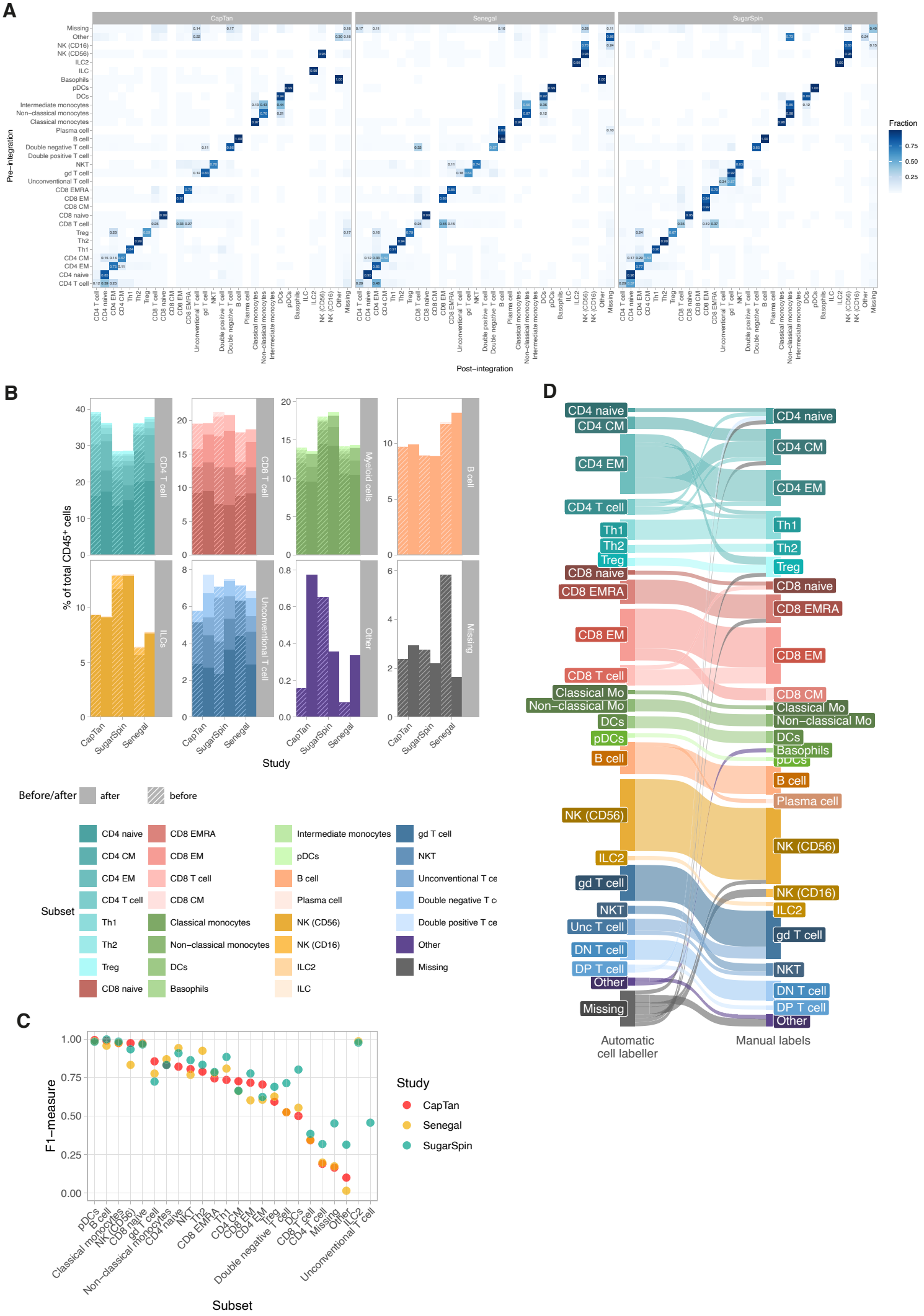
A
CapTan
Senegal
SugarSpin
Pre–integration
Post–integration
Fraction
0.75
0.50
0.25
B
% of total CD45⁺ cells
CD4 T cell
CD8 T cell
Myeloid cells
B cell
ILCs
Unconventional T cell
Other
Missing
CapTan
SugarSpin
Senegal
Study
Before/after
after
before
Subset
CD4 naive
CD4 CM
CD4 EM
CD4 T cell
Th1
Th2
Treg
CD8 naive
CD8 T cell
CD8 EMRA
CD8 EM
CD8 CM
Classical monocytes
Non–classical monocytes
DCs
Basophils
Intermediate monocytes
pDCs
B cell
Plasma cell
NK (CD56)
NK (CD16)
ILC2
ILC
gd T cell
NKT
Unconventional T ce
Double negative T c
Double positive T ce
Other
Missing
C
F1–measure
1.00
0.75
0.50
0.25
0.00
Subset
Study
CapTan
Senegal
SugarSpin
D
Automatic cell labeller
Manual labels
CD4 naive
CD4 CM
CD4 EM
CD4 T cell
Th1
Th2
Treg
CD8 naive
CD8 EMRA
CD8 EM
CD8 T cell
Classical Mo
Non–classical Mo
DCs
pDCs
B cell
NK (CD56)
ILC2
gd T cell
NKT
Unc T cell
DN T cell
DP T cell
Other
Missing
CD8 CM
Basophils
Plasma cell
NK (CD16)

Figure 3

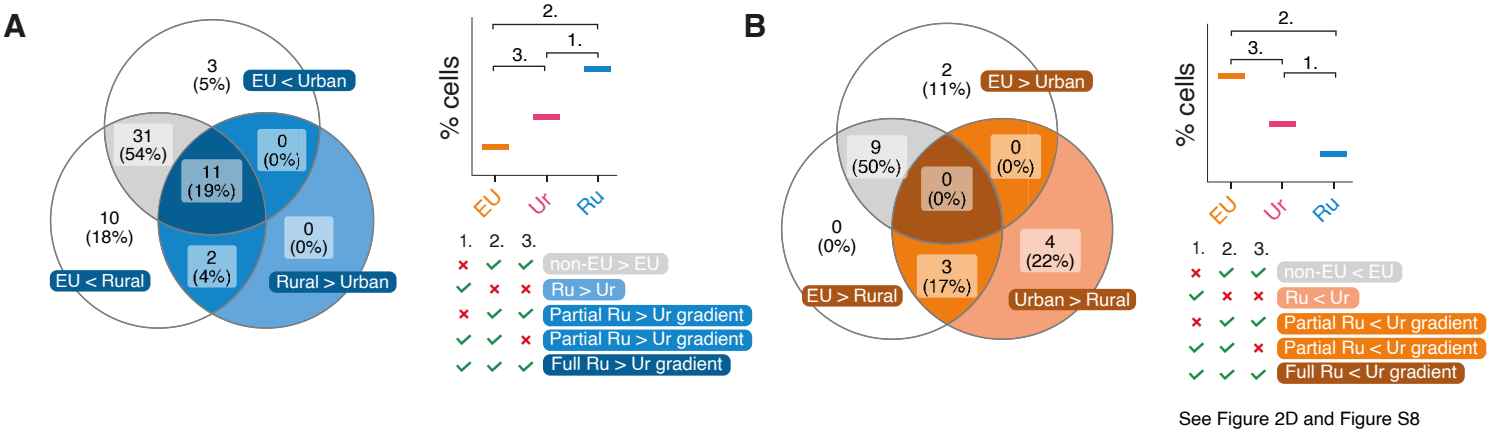
A
3 (5%)
EU < Urban
31 (54%)
0 (0%)
11 (19%)
10 (18%)
0 (0%)
2 (4%)
EU < Rural
Rural > Urban
% cells
EU
Ur
Ru
1. 2. 3.
non-EU > EU
Ru > Ur
Partial Ru > Ur gradient
Partial Ru > Ur gradient
Full Ru > Ur gradient
B
2 (11%)
EU > Urban
9 (50%)
0 (0%)
0 (0%)
0 (0%)
4 (22%)
3 (17%)
EU > Rural
Urban > Rural
% cells
EU
Ur
Ru
1. 2. 3.
non-EU < EU
Ru < Ur
Partial Ru < Ur gradient
Partial Ru < Ur gradient
Full Ru < Ur gradient
See Figure 2D and Figure S8

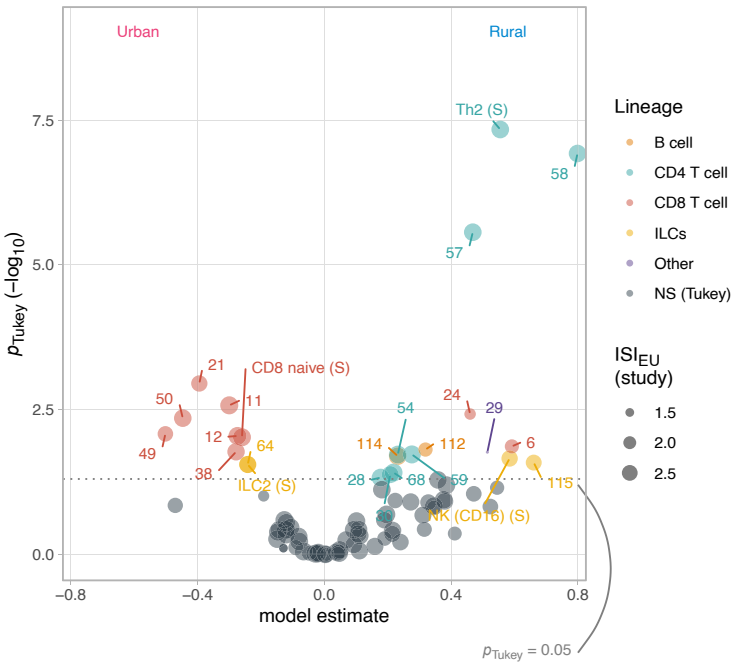
C
Urban
Rural
Th2 (S)
58
57
CD8 naive (S)
21
50
11
49
12
64
38
ILC2 (S)
54
114
112
24
29
6
28
68
59
115
NK (CD16) (S)
p_{Tukey} (−log10)
model estimate
p_{Tukey} = 0.05
Lineage
B cell
CD4 T cell
CD8 T cell
ILCs
Other
NS (Tukey)
ISI_{EU} (study)
1.5
2.0
2.5

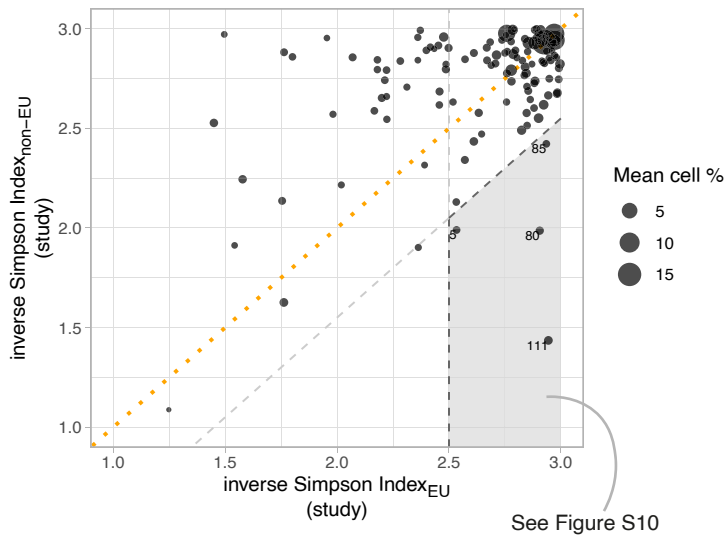
E
inverse Simpson Index non−EU (study)
inverse Simpson Index EU (study)
Mean cell %
5
10
15
See Figure S10

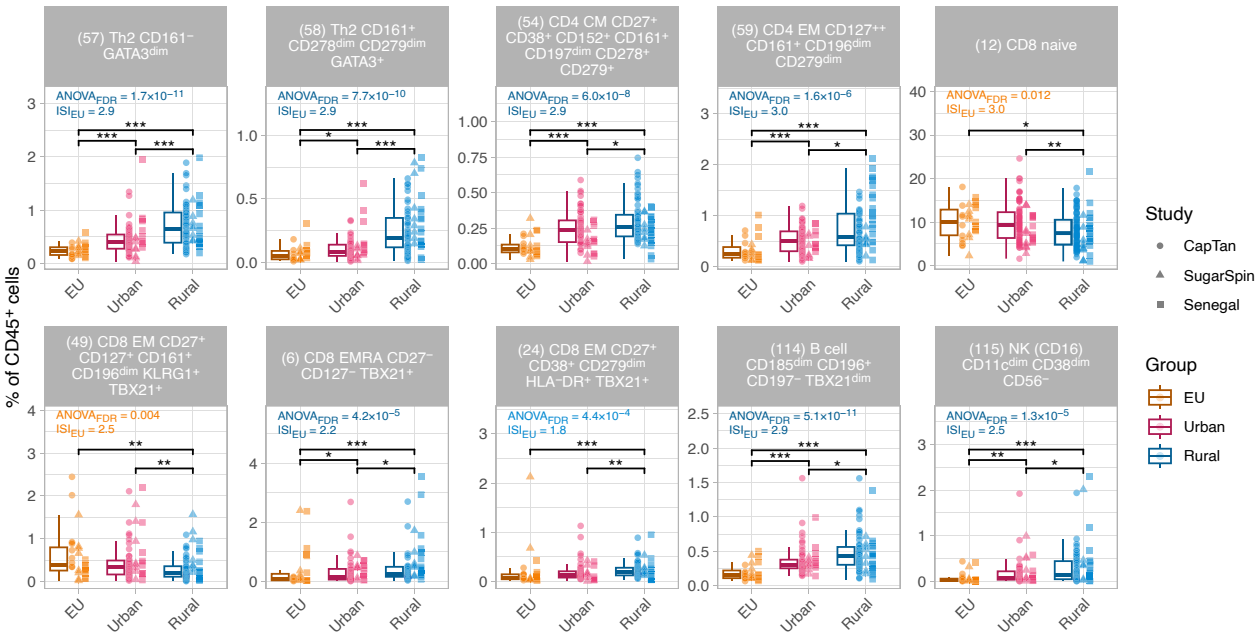
D
(57) Th2 CD161− GATA3dim
ANOVAFDR = 1.7×10−11
ISIEU = 2.9
(58) Th2 CD161+ CD278dim CD279dim GATA3+
ANOVAFDR = 7.7×10−10
ISIEU = 2.9
(54) CD4 CM CD27+ CD38+ CD152+ CD161+ CD197dim CD278+ CD279+
ANOVAFDR = 6.0×10−8
ISIEU = 2.9
(59) CD4 EM CD127++ CD161+ CD196dim CD279dim
ANOVAFDR = 1.6×10−6
ISIEU = 3.0
(12) CD8 naive
ANOVAFDR = 0.012
ISIEU = 3.0
(49) CD8 EM CD27+ CD127+ CD161+ CD196dim KLRG1+ TBX21+
ANOVAFDR = 0.004
ISIEU = 2.5
(6) CD8 EMRA CD27− CD127− TBX21+
ANOVAFDR = 4.2×10−5
ISIEU = 2.2
(24) CD8 EM CD27+ CD38+ CD279dim HLA−DR+ TBX21+
ANOVAFDR = 4.4×10−4
ISIEU = 1.8
(114) B cell CD185dim CD196+ CD197− TBX21dim
ANOVAFDR = 5.1×10−11
ISIEU = 2.9
(115) NK (CD16) CD11cdim CD38dim CD56−
ANOVAFDR = 1.3×10−5
ISIEU = 2.5
% of CD45+ cells
EU
Urban
Rural
Study
CapTan
SugarSpin
Senegal
Group
EU
Urban
Rural

Figure 4

A

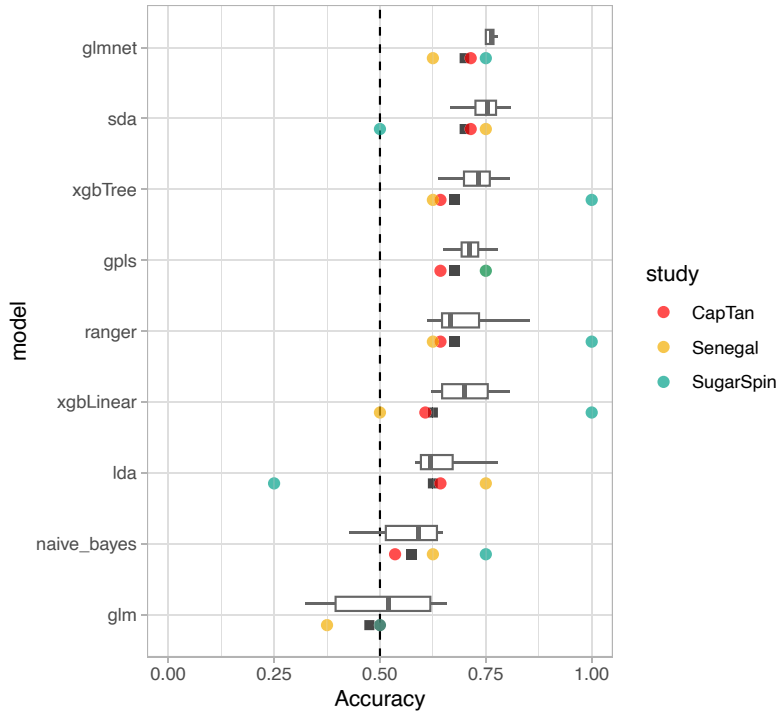
glmnet
sda
xgbTree
gpls
ranger
xgbLinear
lda
naive_bayes
glm
model
0.00
0.25
0.50
0.75
1.00
Accuracy
study
CapTan
Senegal
SugarSpin

B

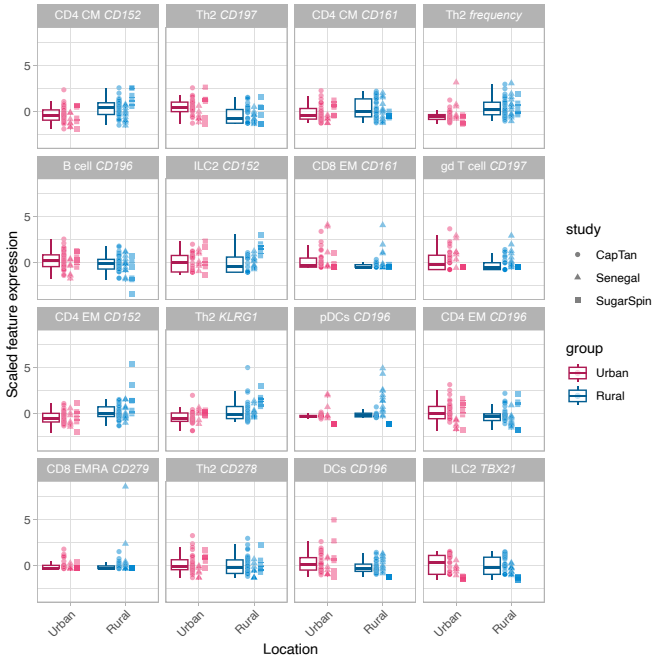
CD4 CM CD152
Th2 CD197
CD4 CM CD161
Th2 frequency
B cell CD196
ILC2 CD152
CD8 EM CD161
gd T cell CD197
CD4 EM CD152
Th2 KLRG1
pDCs CD196
CD4 EM CD196
CD8 EMRA CD279
Th2 CD278
DCs CD196
ILC2 TBX21
Scaled feature expression
5
0
Urban
Rural
Location
study
CapTan
Senegal
SugarSpin
group
Urban
Rural